

UNIVERSITY OF CALGARY

Heat-Assisted and Chemically-Treated Proton Exchange Membrane Electrolysis

by

Hugh Macrae

A THESIS

SUBMITTED TO THE FACULTY OF GRADUATE STUDIES
IN PARTIAL FULFILMENT OF THE REQUIREMENTS FOR THE
DEGREE OF MASTER OF SCIENCE

GRADUATE PROGRAM IN CHEMICAL ENGINEERING

CALGARY, ALBERTA

DECEMBER, 2022

© Hugh Macrae 2022

Abstract

As climate change continues to occur at an accelerating rate, new methods of powering our lives, technologies, and services must be established to achieve environmental stability. Innovative carbon-free methods of energy generation and transportation are necessary to alleviate anthropogenic greenhouse gas contribution. Hydrogen as a chemical energy carrier can manage, store, and transport renewably generated electricity, and function as a portable fuel. For a hydrogen energy platform to displace our current energy platform, hydrogen production, storage, and utilization must become more developed. The purpose of this research will consider the interaction of temperature to improve the efficiency of producing hydrogen via water electrolysis, such that renewable electricity supply in conjunction with low grade heat could be utilized to effectively produce hydrogen. In Alberta, access to low grade geothermal heat for such a process is arguably abundant with the appropriate utilization of the many orphan and inactive oil and gas wells, which offer approximately 90°C downhole. This is an opportunity for companies and institutions who possess or have received the liability of inactive wells. The findings of this research confirm the expected increase in efficiency for hydrogen production under high temperature.

Acknowledgements

A special thanks to Dr. Ian Gates for the much-appreciated opportunity and mentorship to learn about electrochemical hydrogen production and to Dr. Jingyi Wang for his support and guidance throughout the learning process.

Furthermore, this research would not have taken place without the influence of the late Dr. Jon George Pharaoh of Queen's University. Dr. Pharaoh always strived to ameliorate energy systems through his research and introduced me to the bright opportunity of hydrogen as an energy carrier.

Table of Contents

Abstract	ii
Acknowledgements	iii
Table of Contents	iv
List of Tables	vi
List of Figures and Illustrations	vii
List of Symbols, Abbreviations and Nomenclature	viii
CHAPTER ONE: INTRODUCTION	1
1.1 Problem Statement	7
1.2 Research Questions	7
1.3 Organization of Thesis	8
CHAPTER TWO: LITERATURE REVIEW	9
2.1 Electrolysis Literature Review	11
2.2 Solid Oxide Electrolysis Cell	15
2.2.1 HER Electrocatalyst	16
2.2.2 OER Electrocatalyst	16
2.2.3 Membrane	17
2.3 Alkaline Electrolysis	18
2.3.1 HER Electrocatalyst	21
2.3.2 OER Electrocatalyst	22
2.3.3 Membrane	22
2.3.4 Degradation	24
2.4 Proton Exchange Electrolysis	25
2.4.1 OER Electrocatalysts	28
2.4.2 HER Electrocatalyst	33
2.4.3 Membrane	34
2.4.4 Gas Diffusion Layer	41
2.4.5 Degradation	43
2.4.6 Hot-Pressing Assembly	49
2.5 Gaps in Literature	50
CHAPTER THREE: ANALYTICAL MODEL	52
3.1 Models from Literature	52
3.2 Model Development	52
CHAPTER FOUR: EXPERIMENTAL TEMPERATURE AND CHEMICAL TREATMENT EFFECT	66
4.1 Methods and Materials	66
4.1.1 Temperature effect: Results	69
4.1.2 Temperature Effect: Discussion	72
4.2 Chemical Treatment	75
4.2.1 Chemical treatment: Results	75
4.2.2 Chemical treatment: Discussion	76
4.3 Testing Prefabricated Cell	81

4.3.1 Prefabricated Cell Results	81
4.3.2 Prefabricated Cell Disassembly.....	83
CHAPTER FIVE: CONCLUSIONS AND RECOMMENDATIONS	87
REFERENCES	90

List of Tables

Table 2.1: Electrode measurement and modelling techniques.....	14
Table 2.2: OER reaction steps for proton exchange electrolysis known as Krasil'shchikov path (Hansen et al., 2010).....	28
Table 3.1: Heat capacity data for hydrogen, oxygen, and water.....	54
Table 3.2: Enthalpy of formation and Shomate constants.....	55
Table 4.1: Recorded flow rates for the following temperature and applied current to verify the correct reaction is taking place based on Equation (2.1) molar ratio.	69
Table 4.2: List and description of cell components shown in Figure 4.3.2 of the new cell.....	86

List of Figures and Illustrations

Figure 1.1.1: Energy flow diagram of hydrogen's ability to be an energy carrier.	5
Figure 2.4.1: MEA assembly of diagram for PEM. From left to right, the diagram depicts the anode GDL, anode electrocatalyst later, membrane, cathode electrocatalyst, and cathode GDL.	26
Figure 2.4.2: Price chart for platinum (HER) and iridium (OER) (Johnson Matthey, 2022).	30
Figure 3.2.1: Energy demand for HTSE as a function of temperature. As the temperature rises, the amount of electricity required to produce a unit of hydrogen is reduced shown by the dotted line, E (reversible cell potential).	57
Figure 3.2.2: Equivalent circuit for internal impedances of electrolysis cell.	61
Figure 4.1.1: Cathode GDL and copper wire solder connection.	67
Figure 4.1.2: Anode GDL and in-contact with stainless-steel wire.	68
Figure 4.1.3: Temperature effect on the electric potential at onset current and 30mA/cm ² . As well, the electric potential produced from the analytical model for onset current is plotted for comparison.	70
Figure 4.1.4: Electrochemical efficiency of cell with respect to temperature at OCV.	71
Figure 4.1.5: Post treatment cell potential and OCV results with pre-treatment results. .	74
Figure 4.2.1: Post-treatment and pre-treatment OCV faradaic efficiency comparison. ...	76
Figure 4.2.2: MEA [A] is the condition of the MEA before all testing. This MEA has not yet been pressed between the GDLs nor submerged in water. MEA [B] is after the first round of testing.	79
Figure 4.3.1: Performance results with respect to temperature of the new cell and previously in-house tested and built cell.	82
Figure 4.3.2: Image of disassembled cell components of the new cell. See Table 4.2 for description and each component.	85

List of Symbols, Abbreviations and Nomenclature

Symbols	Definition
n	moles
R	gas constant
F	Faraday's constant
E_{cell}	reversible cell potential
E^0	standard reversible cell potential
T	temperature
P	pressure
R_{total}	total resistance
H	enthalpy
S	entropy
G	Gibbs free energy
K	membrane permeability
ρ	density
δ	membrane thickness
μ	viscosity
a	activity
γ	activity coefficient
c	concentration
η	over potential
A	area
Superscript	Definition
c	cathode
a	anode
Abbreviations	Definition
OWA	Orphan Well Association
HTE	High Temperature Electrolysis
SMR	Steam Methane Reforming
GHG	Green House Gas
HTSE	High Temperature Steam Electrolysis
HHV	Higher Heating Value
LHV	Lower Heating Value
STP	Standard Temperature and Pressure
EIS	Electrochemical Impedance Spectroscopy
ASR	Area Specific Resistance
AEC	Alkaline Electrolysis Cell
SOEC	Solid Oxide Electrolysis Cell
PEMEC	Proton Exchange Electrolysis Cell
AEMEC	Anion Exchange Membrane Electrolysis Cell
GDL	Gas Diffusion Layer
MIEC	Mixed Ionic and Electrically Conducting
CFEC	Capillary Fed Electrolysis Cell
HER	Hydrogen Evolution Electrode
OER	Oxygen Evolution Electrode

PDS	Potential Determining Step
CCM	Catalyst Coated Membrane
TFE	Tetrafluoroethylene
PSFA	Perfluorosulfonic Acid
MEA	Membrane Electrode Assembly
CCM-DT	Catalyst Coated Membrane Decal Transfer
CCM-DS	Catalyst Coated Membrane Direct Spray
EW	Equivalent Weight
LSC	Long Side Chain
SSC	Short Side Chain
SPSf	Sulfonated Polysulfone
DSM	Dimensionally Stable Membrane
OCV	Open Circuit Voltage

Chapter One: Introduction

Due to a fluctuating open market of price wars and changing demand for fossil-fuels, Alberta's oil and gas sector has experienced moments of triumph and struggle. Over the past 100+ years, fossil fuel infrastructure has been invested in and established as a reliable system for energy production (in the chemical energy in fuels) as well as energy end-use. An example is the natural gas supply chain which spans from reservoirs to surface facilities to pipelines to municipal distributions networks to building end-consumption. This investment in infrastructure is in the hundreds of billions of dollars and thus, the replacement or adaptation of this infrastructure to low or no emissions energy production and distribution systems will likely require massive investment over the next few decades or more. Thus, there is incentive to seek out low or no emissions energy systems where minimal adaptation of existing systems can take place. In the oil and gas industry, one such infrastructural elements are injection/production wells. Wells represent not only a physical piece of infrastructure but also a liability for oil and gas operators.

As a result of the moments of economic downturn, many companies have had to file for bankruptcy, selling off their tangible assets to their lenders and leaving their liabilities in a state of limbo. These unresolved liabilities are for the most part associated with the costs of decommissioning oil and gas wells in an environmentally friendly manner. For companies that do not plunge into bankruptcy during times of struggle, they remain responsible for providing the necessary funds to cover the liability costs of decommissioning their inactive wells. Inactive wells that do not have an owner and require decommissioning are referred as orphan wells. In Alberta, the Orphan Well Association

(OWA) is a group funded by government and industry to ultimately ensure public safety through the management of environmental risks by facilitating proper decommissioning and land reclamation of orphan wells. As of March 2021, the OWA estimated a total closure cost of the remaining 2,300 orphan wells in the hands of the OWA to range from \$650 million to \$700 million (OWA, n.d.). However, this number does not account for the total inactive and orphaned wells, pipelines, and facilities in Alberta. According to a report published by the Energy Futures Lab in March 2021, there are over 95,000 inactive wells in Alberta, and of those, 7,743 are orphan wells (Alyssa Bruce et al., 2021). This is an enormous public financial and environmental liability. One solution for these wells would be the continued use of them beyond their oil and gas service. In this thesis, the terms orphan well and inactive well are used synonymously as they offer all-year warm environments that can be used for processes.

If a new value stream could be developed for these orphan wells that is profitable, the associated liability would instantly turn into an asset and become a major economic and environmental opportunity. From an economic point of view, orphan wells are considered liabilities since they do not have any value with respect to producing profitable oil and gas. Rather, they have costs for decommissioning and land reclamation. However, all wells contain in-situ geothermal heat in that below a few meters, they always remain above the freezing point. At the bottom of a three-kilometer well, the temperature can be as high as 90°C (Huang et al., 2021). For this reason, one remaining value of these wells lies deep beneath the ground in the form of heat energy. For processes that can utilize this heat could place them ahead of their competition if able to capitalize on the in-situ geothermal heat

especially if on surface, the processes require heat to avoid freezing temperatures – this would include water-based processes. Therefore, if a process can be identified and proven to become more competitive than its competition, by utilizing the thousands of orphan wells, these well assets would no longer be labelled as a liability as they could provide tangible economic value.

One process that can economically benefit from freely available geothermal heat energy is high-temperature electrolysis (HTE) to make green hydrogen production more competitive relative to surface-based electrolysis and steam-methane reforming (SMR) hydrogen production (Todd et al., 2014). In surface-based electrolysis operations in cold climates, a key operational issue is ensuring that the electrolyzers remain sufficiently warm so they do not freeze. The current hydrogen market is 95% supplied by SMR produced hydrogen due largely to the low cost of methane. Hydrogen produced via electrolysis comprises ~4% of the hydrogen market due to electricity costs (IEA, 2020). The current hydrogen market predominately supplies hydrogen as an industrial feedstock.

In addition to Alberta's strong economic relationship with the global volatile oil and gas market, thereby spawning orphan wells and affecting employment in Alberta, domestic oil and gas energy producers are also facing greenhouse gas (GHG) emission costs due to government carbon tax policy. GHG emission costs have been implemented to promote the transition away from high GHG emitting processes providing incentives towards processes that are clean (low or zero GHG emissions). This means as demand increases for lower GHG emission energy and chemicals, renewable electricity grid supply and clean portable

fuels will become more and more necessary. However, as societies transition to cleaner energy platforms, new challenges of managing and storing energy arise. Due to the uncontrollable nature of wind patterns and sun exposure, renewable energy supply is at the mercy of weather. To bridge the disconnect between an uncontrollable energy supply and society's somewhat predictable energy demand, grid scale energy storage is necessary to store and discharge energy during moments that renewable generation exceeds or fails to meet the grid demand of electricity. Hydrogen can serve as an energy carrier and storage medium with the utilization of an electrolysis cell and a fuel cell, for the effective deployment of renewable generation and for the effective displacement of carbon-based fuels for transportation and machinery. Hydrogen produced by water electrolysis is considered as a strong energy carrier technology option to adjust the balance between the generation of power source by renewable primary energy and energy demand for end-use (Wang et al., 2014). An electrolysis cell, similar to a fuel cell, is an energy conversion device that converts electrical energy (electricity) into chemical energy (hydrogen and oxygen) and heat. Furthermore, hydrogen can also serve as a portable chemical fuel to displace many current fossil-fuel technologies, namely, long-haul modes of transportation (i.e. planes, ships and trains). These two emerging hydrogen supply chains could provide opportunity for current energy producers to diversify into a new efficient net-zero energy platform.

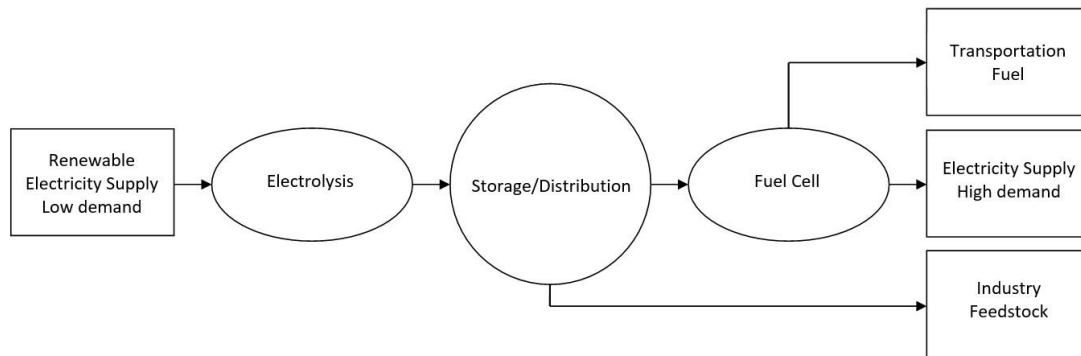


Figure 1.1.1: Energy flow diagram of hydrogen's ability to be an energy carrier.

Hydrogen electrolysis using heat to lower the electricity required to dissociate the water molecule has been studied for over 40 years. The first in depth study of high temperature steam electrolysis (HTSE) was in 1979 by Doenitz et al., which effectively outlined both thermodynamic and electrochemical efficiencies (Doenitz et al., n.d.). Similar to conventional electrolysis cells, voltage is applied to two electrodes exposed to water such that hydrogen and oxygen are evolved at their respective electrodes. The innovation with HTE considers heat as an additional input along with electricity to decompose the water molecule into the respective hydrogen and oxygen molecules. They also discussed the challenges the technology faced for producing hydrogen in large quantities and at high temperatures, many of which are transport and material fatigue problems. The early research did not lead to any significant innovations since hydrogen generation and use quickly lost momentum as costs were high relative to fossil fuels. However, a few decades later, when scientists and governments began to recognize the threat of climate change, research towards hydrogen technology was sparked again due to the forecasted demand for a clean large scale energy (IEA, 2019). More research has led to more effective electrodes,

electrolytes, and ion conductive membranes – all serving to raise the efficiency and saving electricity consumption.

The amount of energy that results from the electrolysis cell is encapsulated in the form of hydrogen and the amount of energy it contains. This considers the notion that an electrolysis cell is an energy conversion technology such that heat and electricity can be converted into chemical energy. This amount of energy that hydrogen can store is typically reflected by the higher heating value (HHV) of hydrogen which is equal to 285.84 kJ/mol of hydrogen (Kumar and Himabindu, 2019). This is chosen because the HHV considers the latent heat of the water. Including the latent heat consumption is necessary since the water after the hydrogen is spent, via a fuel cell, is assumed to return to liquid phase. A fuel cell is used to exploit the energy that is stored in the hydrogen by converting the chemical hydrogen energy into electricity and heat. While the lower heating value (LHV) of hydrogen does not account for the latent heat and is used for systems where the water leaving the fuel cell (i.e. spent hydrogen) is assumed to remain in the vapour phase. Returning to focus back to the electrolysis cell, the two forms of energy inputs for this process are a combination of electrical energy and thermal energy. The thermal energy is necessary to minimize the amount of electrical energy since electricity costs comprise ~80% of producing hydrogen via electrolysis (Mingyi et al., 2008). Additionally, the increased thermal energy within the system also improves ion transport through the electrolyte. For this reason, it is critical to understand the electrical and thermal energy inputs to whilst striving towards high efficiency and low operating cost electrolysis.

Major barriers stand in the way of hydrogen's ability to capture these new emerging energy carrier markets, such that the production, storage, distribution, and utilization of hydrogen must all become developed. This study will focus on the production segment and examine whether geothermal assisted hydrogen electrolysis can compete with the current hydrogen production market, and if not, outlining the remaining barriers.

1.1 Problem Statement

To assist the transition of renewable and other low emission (i.e. green) energy generation technologies, energy storage and carbon-neutral fuels must be developed to integrate the continuation of technologies and services that our society use today and that the next generation of green energy generations methods cannot directly support. As aforementioned, hydrogen can fill this gap. The current barriers that hydrogen faces to fill the described gap and to support such a transition includes high capital and operating costs to produce, store, transport, and consume hydrogen relative to the costs involved with our current technologies and services that need to become carbon-neutral and that green energy generation cannot directly replace. In the research conducted and documented in this thesis, the effect of temperature on liquid phase electrolysis of water is explored. If warm or hot environments are used for the production of hydrogen via electrolysis, then there may gains of efficiency that improves process economics and acceptability.

1.2 Research Questions

Major barriers stand in the way of hydrogen's ability to capture these new emerging energy carrier markets, such that the production, storage, distribution, and utilization of hydrogen must all become developed. This study will focus on the production segment and examine the effect of temperature to simulate how geothermal heat can assist hydrogen electrolysis. The second set part of this study considered the effect of chemically treating the titanium anode gas diffusion layer to determine whether a titanium dioxide passivation layer was present, thus contributing to the poor performance. The research questions that are answered in the research conducted and reported in this thesis are as follows:

1. How much does temperature reduce electricity consumption for electrolysis of water for generating water?
2. Is there a titanium dioxide passivation layer contributing to poor performance?

1.3 Organization of Thesis

This thesis consists of five chapters as outlined as follows. **Chapter One** introduces the research background, research questions and outline of the thesis. **Chapter Two** presents a literature review of current hydrogen electrolysis production methods with focus on proton exchange membrane electrolysis. **Chapter Three** describes the analytical model of cell potential as a function of temperature, which correlates electricity consumption. **Chapter Four** presents the experimental findings of temperature effect and chemical treating the anode GDL on the performance of the cell. **Chapter Five** lists the overall conclusions from the research conducted and provides recommendations for future research.

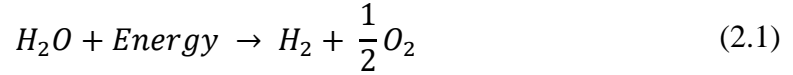
Chapter Two: Literature Review

There are many pathways to produce and/or synthesize hydrogen either electrochemically, thermochemically or biologically. The literature considered for this research involves electrochemical hydrogen production methods, such that electricity is a necessary input. These processes involve passing current and voltage through a water electrolysis circuit to dissociate water into hydrogen and oxygen. The current applied to the system corresponds to the rate at which the electrons are supplied to split water into hydrogen and oxygen whereas the voltage is responsible for generating the necessary electrochemical charge difference between the electrodes to overcome the intermolecular forces holding water together, corresponding to the positively charged hydrogen ion and negatively charged oxygen or hydroxide ion, depending on the catalyst used.

Green hydrogen production methods have low direct or trace GHG emissions whereas steam-methane reforming (SMR) generates large GHG emissions. Currently 96% of the hydrogen produced today is supplied via SMR and therefore, this is used as an economic benchmark (Wang et al., 2014). According to Ayers et al., the United States Department of Energy (DOE) target of 2 A/cm^2 at 1.5 V is equivalent to \$2 per kg of H_2 (Ayers et al., 2012). This corresponds to the lower pricing range of \$2-4 per kg of H_2 for electrolysis to become competitive with fossil fuel produced hydrogen (Spöri et al., 2017).

Electrolysis uses electricity to dissociate water into oxygen and hydrogen. Fundamentally, with the addition of external heat, the reaction can proceed by consuming less electricity

compared to the case of no external application of heat. This behaviour indicates that the applied energy can come in the form of either electricity, heat or a combination which can be represented by:



The purpose of applying external heat to the electrolysis cell is to reduce the operating costs by consuming less electricity (expensive form of energy) and more low-grade heat (inexpensive form of energy). In addition, because the conversion efficiency of heat to electricity is low compared to using heat directly, the total energy efficiency can be increased if the heat can be used directly from the heat source (Mansilla et al., 2007). However, electricity remains necessary for all low-grade heat sources since the Gibbs free energy change of splitting water becomes negative at approximately 2500K (Rozain and Millet, 2014). For this reason, from thermodynamic principles, electrolysis can economically benefit from naturally occurring high temperature environments. Examples of such environments include volcanic systems, hot pools, deep underground geothermal resources, and solar-irradiated surface locations such as deserts (during the daytime).

Publications in the literature on water electrolysis were investigated to outline recent electrochemical material advances. These recent advancements focus on lowering the electrochemical overpotential of the hydrogen and oxygen evolution reactions, which corresponds to the operating costs, while also lowering the amount of catalyst used per area, which corresponds to the capital costs.

2.1 Electrolysis Literature Review

In general, water electrolysis is the process of using electricity to split water into hydrogen and oxygen. Electricity is necessary to impose the required charge difference across the electrodes as an electrical force to split water. There are three main types of water electrolysis cells that are currently popular: solid oxide electrolysis cells (SOECs), alkaline electrolysis cells (AECs), and proton exchange membrane electrolysis cells (PEMECs or PEMs). In addition, more recently, a new emerging cell takes the disadvantages and advantages of the AEC and PEMEC, respectively, and is called an anion-exchange membrane electrolysis cell (AEMEC). The basic premise of all the cells is consistent: electricity is required to provide the necessary applied energy to overcome the intermolecular forces of the water molecule to split it into its elemental components hydrogen and oxygen. In addition, through time, the design characteristics of all the cells have evolved towards reducing the electricity consumption while maximizing the gas yield and ensuring material durability for long-term dynamic operation.

Research efforts can be broken down into studying the electrical and ionic conductivity, gas/liquid transport, and electrocatalyst performance which is often targeted towards identifying the specific limiting step in the process. These behaviours can be measured in terms of equivalent impedances to differentiate and assess the ohmic, ionic, kinetic, and catalytic phenomena. Other aspects of these systems that are examined are methods to reduce the electricity consumption which is linked to the operating cost, the expense of the

materials used in the system (reflects the capital cost of the system), the degradation of the materials within the systems (relates to the replacement capital costs), and operational conditions of the systems, for example, whether in hot or cold climate locations. In general, the cumulative effort that has been advanced among the various methods of electrolysis has targeted the reduction of the specific electricity consumption (i.e. operating cost), degradation rate (i.e. maintenance/replacement cost), and associated capital (i.e. material cost) to ultimately promote hydrogen as an energy storage carrier and portable fuel option.

Electrocatalysts play a critical role since they can be considered as the starting point for such electrochemical reactions and are responsible for splitting the water into the desired intermediate ion. The intermediate ion for the SOEC, AEMEC, and PEMEC is O^{2-} , OH^- , and H^+ , respectively. The three different cells are critically different such their electrocatalysts and membrane are highly selective at generating and conducting their respective intermittent ion, and are designed to restrict all other liquid, ionic, and/or gas compounds as much as possible. Furthermore, the electrocatalysts often consist of rare and expensive materials due to the nature of which elemental combinations display effective binding energies towards the desired intermediate; this is especially the case for PEMECs (Rossmeisler et al., 2007) and SOEC (Yu et al., 2008). AEMECs offer more common metal electrocatalysts that are suitable for hydroxide formation, ultimately reducing capital costs (Buttler and Spliethoff, 2018). To reduce the capital cost associated with electrode materials, other materials known as supports are introduced into the design to increase the specific surface area of the catalyst. Effective support materials share similar molecular crystallinity to the catalyst for effective contact and offer very high

internal specific surface area to effectively provide a large coating surface for the catalyst. As a result of this restrictive relationship between the compatibility of the support and catalyst materials, careful consideration is carried out for effective cell performance. Buttler and Spliethoff (2018) summarized a list of the current electrolysis cell manufacturers, including their respective I-U curve specifications for SOEC, AEMEC and PEMEC (Buttler and Spliethoff, 2018).

In general, the goal of designing effective electrocatalysts, GDLs, and membranes involve the selection of materials that maximize interfacial surface area, ensure high corrosion resistance, exhibit high electrical and ionic conductivity, have reasonable costs by avoiding scarce elements, demonstrate reasonable lifetime, and possess low activation overpotentials/resistances (i.e., low Tafel-slope) (Santos et al., 2021). These characteristics are analyzed using the various devices and modelling methods, outlined in Table 2.1, to understand electrochemical properties. Furthermore, since these reactions are multiphase involving gas and liquid, electrode materials must be highly porous and possess highly hydrophilic surfaces for effective gas transport and minimal bubble interface coverage on the surface of the electrode (Rashid et al., 2015; Wang et al., 2014).

In general, the cumulative research effort that has been advanced among the various methods of electrolysis has targeted the reduction of the specific electricity consumption (i.e., operating cost), degradation rate (i.e., maintenance/replacement cost), and associated capital (i.e. material cost) to ultimately promote hydrogen as an energy storage carrier and portable fuel option.

Table 2.1: Electrode measurement and modelling techniques.

Measurement Device / Modelling Method	Purpose/Description
Electrochemical Impedance Spectroscopy (EIS) Cyclic-Voltammetry (CV)	Properties of electrochemical system through the lens of impedance. EIS uses sinusoidal voltage perturbations, small departures from the equilibrium at different time scales, can be identify (i.e. ohmic resistances, charge transfer resistances, double layer capacitance, inductance from wiring etc.) The frequency of the applied potential is altered throughout the measurement to analyze different impedance contributing phenomenon that either occur on small or large relative time scales (Li et al., 2019; Rozain et al., 2016b).
Cyclic-Voltammetry (CV)	Number of electroactive sites on electrode surface available. The working electrode potential is ramped linearly versus time, once the set potential is reached, the working potential is ramped in opposite direction to return to initial potential. The amount of charge measured is proportional of the true area of the electrode interface (Millet et al., 2011; Zhao et al., 2015).
Scanning Electron Microscope (SEM)	Produces images of a sample by scanning the surface with a focused beam of electrons, which describe the morphology (Kadokia et al., 2012; Zhao et al., 2015).
X-Ray Diffraction (XRD)	Analysis to describe the phase purity and crystalline structure for electrocatalysts (Kadokia et al., 2014; Siracusano et al., 2014).
X-Ray Photoelectron Spectroscopy (XPS)	To identify chemical elements and surface composition of electrocatalysts (Karimi & Peppley, 2017; Lv et al., 2019).
Rotating Ring Disk Electrode (RRDE)	Obtaining information about catalyst selectivity, reaction kinetics and detailed impedance contribution mechanisms of the electrochemical reaction (Kadokia, 2014) Additionally, offers method to validate catalyst activity (Neyerlin et al., 2009).
Brunauer-Emmett-Teller (BET)	Describes the physical adsorption of gas molecules on a solid surface as a technique to measure the specific surface area of materials (Karimi and Peppley, 2017).
Energy Dispersive X-Ray Spectroscopy (EDS)	Elemental mapping technique to confirm construction of microscopic particles in separators/membranes (Lee et al., 2020).

2.2 Solid Oxide Electrolysis Cell

The solid oxide electrolysis cell (SOEC) is widely recognized as the only electrolysis method for very high temperatures offering high thermodynamic efficiencies (Yu et al., 2008). Other electrolysis cells have temperature ceilings around 90°C (Marcelo Carmo, 2013) to operate with liquid water, whereas the SOEC operates at very high temperatures such that superheated steam (600-1000°C) is fed as the reactant. The innovation with this cell involves the ability to operate with superheated steam, instead of operating with liquid water reactant, such that the membrane and electrodes are thermally stable to remain unchanged when under these high temperatures (Doenitz et al., n.d.).

As aforementioned, increasing the temperature reduces the reversible cell potential due to conservation of energy inputs. Increasing the temperature also promotes the kinetics of the reaction such that transport resistances are reduced (Shin et al., 2007). The innovation with this cell facilitates the pursuit towards the lowest reversible cell potential, outlined by the Nernst equation, by operating at very high temperatures, typically paired with heat reactors for low-cost high temperature steam supply (Fujiwara et al., 2008) or high temperature geothermal source (Sigurvinsson et al., 2007).

Despite its high efficiency and low relative electricity consumption, the SOEC does not satisfy the operating conditions of orphan/inactive oil and gas wells due to their lower temperature conditions which are insufficient for effective SOEC operation. As a result of this constraint, the SOEC was not considered for experimental testing in this research since

the AEMEC and PEMEC can operate at lower temperatures, i.e., up to $\sim 90^{\circ}\text{C}$, instead of the required minimum temperature of 600°C for SOEC (Babic et al., 2017). For other applications that possess an abundance of very high temperature superheated steam, the SOEC is an appropriate candidate (O'Brien, 2012).

Furthermore, SOECs offer the ability to operate in a co-electrolysis mode to convert water vapour and carbon dioxide gas into hydrogen and carbon monoxide gas, respectively (Reytier et al., 2015). This is an alternative and attractive route as it converts sequestered CO_2 into CO for fuel conversion.

2.2.1 HER Electrocatalyst

The hydrogen electrode is constructed using a nickel based YSZ cermet (a cermet is a heat-resistant material made of ceramic and sintered metal). The nickel offers high electric conductivity and catalytic activity; however nickel alone suffers from aggregation at high temperatures. For this reason, it is common for the electrolyte, commonly YSZ, and nickel to be introduced as a cermet (Sato et al., 2021).

2.2.2 OER Electrocatalyst

The oxygen electrode is of particular interest for SOEC performance since it contributes a large extent to the cell polarization resistance. The use of a mixed ionic and electric conducting (MIEC) oxygen electrode is necessary since they extend the reaction zones, thereby reducing the polarization associated with activation resistances (Chauveau et al.,

2011). Commercially available SOECs typically include Sr-doped LaMnO₃ (LSM), which is a perovskite-structured oxygen electrode. Perovskites are a common material for oxygen electrodes due to their high oxygen outer coverage, which facilitate either the dissociative or associative oxygen evolution pathway (Beall et al., 2021). Developments concerning other perovskite element combinations have been studied, of which demonstrate increased performance relative to conventional LSM. Chauveau et al. demonstrated increased performance of both La₂NiO_{4+δ} and Nd₂NiO_{4+δ} in terms of reduced area specific resistance (ASR). Bo et al. determined a novel oxygen catalyst, Ba_{0.5}Sr_{0.5}Co_{0.8}Fe_{0.2}O_{3-δ} (BSFC), which offered a significantly lower ASR for low and high current densities, and for fuel cell operating mode, compared to the conventional LSM catalyst (Bo et al., 2010).

2.2.3 Membrane

First demonstrated by Doentiz et al. in 1980, the SOEC is based on an oxygen ion conducting solid ceramic electrolyte of yttria (Y₂O₃ mole fraction 8%-12%) stabilized zirconia (ZrO₂) (YSZ), which was reported to remain unchanged in composition during HTSE (Doentiz et al., n.d.). Around the same time, Westinghouse Electric Co. took these findings and developed a calcia stabilized zirconia (CSZ) (Yu et al., 2008). More recently, Osada et al. tested the SOEC performance with a scandia stabilized zirconia electrolyte (SSZ) (Osada et al., 2006). These membranes all offer the selective transport of O²⁻ ions while restricting gas crossover. Aicart et al. noted crossover in fuel cell mode, which was determined based on unexpected temperature gradients due to hydrogen and oxygen mixing (Aicart et al., 2022). The identified temperature gradients between cells increased

in polarization during higher production rates, concluding crossover is present and is exacerbated with increased current density. This crossover and current density relationship is congruent with AEMEC and PEMEC designs. Crossover as a design and operation concern is reported much less for SOECs relative to PEMECs, likely due to the single-phase (i.e. gas only) nature of SOEC.

2.3 Alkaline Electrolysis

The cheapest and most accessible method of electrolysis is done using an alkaline liquid water electrolyte between two electrodes such that hydroxide ions are the conducting ion. This cell typically uses a 20-40 wt.% potassium-hydroxide (KOH) solution as the liquid electrolyte. However, Allebrod et al. more accurately determined that a 30-34% wt. KOH concentration is optimum (Allebrod et al., 2012). The alkaline electrolysis cell (AEC) is the cheapest, in terms of capital cost (Santos et al., 2021), and most accessible method of electrolysis due to the relative abundance of permittable electrode catalyst materials, such that they split water into hydroxide ions. Since most non-noble transition metals will promote hydroxide ions, in addition to expensive noble transition metals, electrocatalyst selectivity is less of a challenge for AECs. More accurately, the permittable non-noble transition metal electrode materials include nickel, chromium, cobalt, iron, zinc, or molybdenum (Pletcher and Li, 2011). Of these metals, nickel is the most active non-noble transition metal that demonstrates stability in an alkaline medium, and is abundant, making it typically the preferred choice and most common electrode-based element (Gong et al.,

2016). Further discussion involving electrode specific electrocatalyst materials are discussed in the following sections.

Since the alkaline electrolyte solution is not guaranteed to be compliant with the cell design in that leakage may occur since components of the cell casing may corrode when exposed to the alkaline solution, thereby creating contamination issues down the road. Despite the favourable characteristics of non-noble transition metal electrocatalyst eligibility, the AEC was not considered further due to the required highly alkaline water solution and inability to effectively perform under high pressure.

Promisingly however, current research has been concerned with the drawbacks of maintaining the highly alkaline liquid water electrolyte to facilitate hydroxide formation and ion transport. These recent research efforts involve developing an AEC without usage of highly concentrated liquid electrolyte (i.e., 30 wt.% KOH), but instead, operates with dilute electrolyte (i.e., 3 wt.% KOH) and maintains the use of non-noble transition metals (Vincent et al., 2021). This combination could become realized by the development of a suitable anion-exchange membrane electrolysis cell (AEMEC) to permit hydroxide ion transport and the use of dilute alkaline electrolyte water. Unfortunately, there is no anion-exchange membrane (AEM) material that clearly satisfies performance and stability for AEMEC (Brauns et al., 2021), indicating that the technology is still developing. Published performances of AEMs are discussed in Section 2.3.3. Millet et al. performed a review of this concept finding a mere 20 papers published between 2012 and 2019 (Miller et al., 2020), further indicated the technology is in early development.

Alternatively, Hodges et al. developed a capillary fed electrolysis cell (CFEC) that uses an alkaline electrolyte solution along with non-noble transition metal electrocatalysts to deliver high purity gas at nearly 100% efficiency (Hodges et al., 2022). The basis of their design revolves around a unidirectional electrochemical flow process. This means the reactant and products flow in one direction through the cell, in contrast to existing electrolysis cells, which consist of a counter-current flow behaviour of liquid and gas species. As a result of the unidirectional characteristic, bubble formation and interference effect is not an issue since water is converted directly to the bulk gases without bubble formation. Furthermore, advective gas crossover is not a possibility for a CFEC since the gas and liquid electrolyte are never in contact. Furthermore again, diffusion gas crossover is drastically reduced due to the high molarity alkaline electrolyte thereby only permitting a small amount of crossover.

Moreover, AECs possess the ability to function with the utilization of seawater, such that saline water electrolysis is more favourable in alkaline than acidic conditions, illustrated by the associated Pourbaix diagram (Fukuzumi et al., 2017). Amikam et al. studied the use of NaOH as the AEC electrolyte with the intention to precipitate out the aqueous NaCl to negate the production of chloride gas at the anode (Amikam et al., 2018). They determined that an aqueous NaOH concentration of 100g/kgH₂O or more, contributed to absolutely no chlorine production, indicating that all the NaCl precipitated out of the seawater solution. This is a challenge worth pursuing since seawater is much more abundant than freshwater (i.e. water with little impurities), however the difficulty of seawater electrolysis considers

the favourability of the chlorine evolution relative to the oxygen evolution reaction (Fukuzumi et al., 2017). The discrepancy between these reactions considers the two-electron transfer for chlorine compared to the 4-electron transfer for oxygen, thus promoting chlorine gas instead of oxygen gas as the anode product for seawater electrolysis (Tong et al., 2020). In addition to chlorine being a toxic and corrosive towards the catalyst and substrates, the amount of chlorine gas that would be produced relative to the amount of hydrogen produced far exceeds the chlorine gas market demand (Kuang et al., 2019). Kuang et al. proposed an alternative route to promote the OER in NaCl-containing solution (i.e. seawater equivalent), which considered an innovative corrosion-resistant and OER selective catalyst (Kuang et al., 2019). Their work attempted to improve Mn-based oxides deposited onto IrO₂-Ti (El-Moneim, 2011) and NiFe-layered double hydroxide (Tong et al., 2020). However, the materials lacked long-term stability at current densities greater than 1 A/cm². They also developed a multilayer NiFe/NiS_x-Ni foam electrode which demonstrated higher OER activity and corrosion resistance (Kuang et al., 2019).

2.3.1 HER Electrocatalyst

A negative potential is present at the hydrogen evolution reaction (HER) electrode, allowing metallic nickel to be the stable form in alkaline solution, indicated by the Pourbaix diagram for nickel. However, bare nickel presents too large of an overpotential for modern electrolyzer standards (300-400mV), such that nickel foams offer a higher activity due to the increased specific surface area (Santos et al., 2021). Furthermore, combining other transition metals to a nickel foam support has shown significant improvements and reduced

overpotential losses (Sapountzi et al., 2017). Raj and Vasu determined that Ni-Mo binary electrocatalyst offered the best corrosion resistance, and stability for both open circuit and increased current operation against all the alloys tested (Raj and Vasu, 1990). Other tested alloys in the order of most to least activity were Ni-Zn > Ni-Co > Ni-W > Ni-Fe > Ni-Cr. The same group went onto studied tertiary Ni-based electrocatalysts, such that all the tertiary combinations include molybdenum as a participant and show similar performance to the binary Ni-Mo while reducing the loading of molybdenum.

2.3.2 OER Electrocatalyst

For the oxygen evolution reaction (OER) electrode, a positive potential is applied causing nickel oxide (NiO) and/or nickel (oxy)hydroxide (NiOOH) to be the stable forms of nickel such that it does not corrode, as illustrated in the Pourbaix diagram for nickel (Santos et al., 2021). Interestingly, Trzeźniewski et al. carried out a spectro-electrochemical study of a NiFeOOH electrocatalyst for the OER and found that the surface gets charged before the reaction starts, such that, the negatively charged sites act as OER precursors (Trzeźniewski et al., 2015). These oxides can be electrocoated onto a Ni wire mesh to function as the anode, or even better, a Ni foam to provide a higher specific surface area.

2.3.3 Membrane

To maximize the production yield, maintaining appropriate gas separation between the two electrodes is necessary. Gas crossover reduces the purity of the produced gases which reduces the overall effectiveness of the cell and introduces safety concerns with respect to

hydrogen combustion when exposed to oxygen (Miller et al., 2020). To mitigate gas crossover effects, a membrane material is placed in-between the two electrochemical electrodes to function as a gas separator and conduction medium for the intermediate ion. A commonly used alkaline electrolysis membrane (AEM) is Zirfon™ Perl UTP 500, which is known for low gas contamination and high ion conductivity (Schalenbach, Lueke, et al., 2016). Moreover, Lee et al. characterized a cerium oxide-polysulfone composite separator that out-performed the Zirfon™ Perl separator in terms of ohmic resistance and hydrogen permeability (Lee et al., 2020). According to Fernandez et al., the most common AEMs are Fumasep® FAA-3, Sustainion® 37-50, Tokuyama A201, Aemion™ and Orion™ (López-Fernández et al., 2021).

Liu et al. studied the performance and stability of various other different AEMs, such that Sustainion® 37-50 demonstrated 1000 mA/cm² at 1.9V for 2,000 hours in a 1M KOH solution (Liu et al., 2017). This group tested other membranes although they showed significantly worse performance and stability, which considered Fumasep® FAS-50, Fumasep® FAPQ, Neoseta ACM, AMI 7001, Nafion® 115 and Celazole® PBI. Furthermore, Sustainion® 37-50 had the lowest ASR at 60°C and highest ion conductivity, and demonstrated an increasing ion conductivity with temperature up to 80°C.

Unfortunately, since the working electrolyte (i.e., aqueous KOH) for AECs is liquid phase, and functions by permeating hydroxide transport through the separator to conduct ions, differential pressure operation is not recommended to avoid gas crossover (Sapountzi et al., 2017). Gas crossover during differential pressure operation is due to the saturation of

hydrogen and oxygen gas in the liquid electrolyte such that when electrolyte and gas saturated water pass through the separator due to the pressure difference, it carries gas with it, known as advective flow. Furthermore, aside from the associated concerns of gas yield efficiency and safety due to gas crossover, separator degradation is enhanced during differential pressure operation due to enhanced unwanted gas blockage (Sapountzi et al., 2017). As a result of these phenomenon, high pressure AEC operation is not recommended. However as aforementioned, AEMECs have the potential to maintain product gas separation and accommodate non-PGM catalysts but due to the limited publications it was not considered for further testing at this time.

2.3.4 Degradation

Buttler and Spliethoff (2018) summarized recent reports of AEC degradation rates, such that they offer similar and/or lesser rates of degradation compared to PEMEC. It should be noted that when comparing the rates of degradation between different cells, the initial performance should be considered. As a result of this, a PEMEC with a slightly larger degradation rate relative to a AEMEC will still outperform in terms of I-U curve performance (Buttler & Spliethoff, 2018).

Felgenhauer and Hamacher (2015) outlined typical stack degradation rates and operating lifetimes for commercial AECs, and PEMs for comparison (Felgenhauer and Hamacher, 2015). Their evaluation of commercial AECs revealed lifetimes ranging from 6 to 11 years

and with an average degradation rate of 0.25 to 1.5% per year whereas PEMs offered slightly greater lifetimes, similar degradation rates, but higher capital costs.

Another degradation mechanism specific to AECs considers the formation of K_2CO_3 precipitates when ambient CO_2 is present, from dissolving into the electrolyte (López-Fernández et al., 2021). These precipitates then clog the pores of the anode gas diffusion layer (GDL), thus reducing the functioning electrochemical cell area.

2.4 Proton Exchange Electrolysis

A proton exchange membrane (PEM) is polymer-based membrane that permits the transport of hydrogen ions, as illustrated in Figure 2.4.1. These ions transport through the membrane via electrical force, by concentration and pressure gradients (Schalenbach et al., 2013). The innovation associated with a proton exchange membrane electrolysis cell (PEMEC) considers high selectivity (i.e. low gas crossover), high proton conductivity and high current density operation (i.e. low resistances), compact stack design, dynamic range operation, and high pressure operation (Kadokia et al., 2014). These promising attributes are due to the compact solid nature and highly selective and highly conductive proton exchange material. Furthermore, the PEMEC does not require the usage of highly corrosive alkaline feed water, instead it uses pure water (Ayers et al., 2012). This is an important characteristic in terms of environmental considerations and balance of plant when performing electrolysis deep underground and in remote locations.

The solid nature and high ion conductivity of the dual functioning ion conducting electrolyte and gas separating PEM allows the system to have a quicker start-up and more dynamic operation, making it a suitable candidate for variable power load applications, compared to AECs (Sapountzi et al., 2017). Moreover again, the solid electrolyte permits compact cell configuration that is suitable for confined spaces that offer high temperature and high pressure (Kadokia et al., 2014).

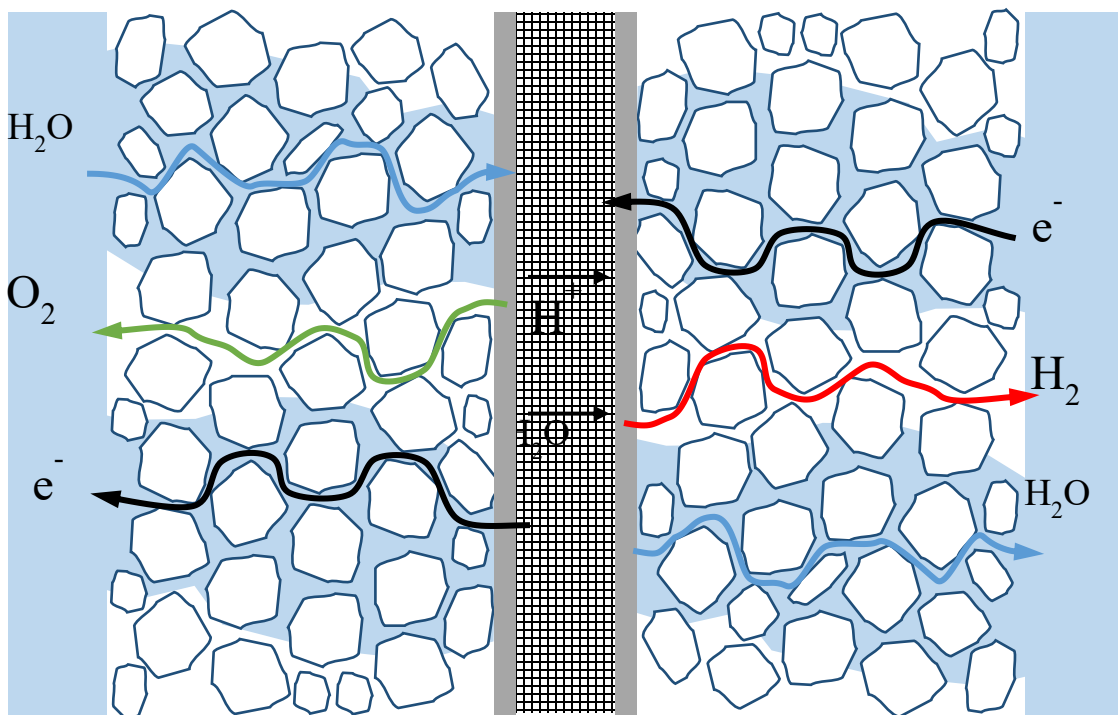


Figure 2.4.1: MEA assembly of diagram for PEM. From left to right, the diagram depicts the anode gas diffusion layer (GDL), anode electrocatalyst layer, membrane, cathode electrocatalyst, and cathode GDL.

The porous transport layer (PTL), otherwise referred to as the gas diffusion layer (GDL), allows for the transmission of current from the bi-polar plates to the catalyst layers on either side of the membrane and transport of reactants/products.

Drawbacks to PEM electrolysis involve utilizing rare materials that are sufficient to withstand the highly acidic environments due to the high concentration of hydrogen ions. Furthermore, at the anode where the OER takes place, electrochemical activity is poor resulting in sluggish kinetics. Millet et al. outlined the ratio of the exchange current density for H^+/H_2 on the most effective cathodic catalyst for HER in acidic media (metallic platinum) to the exchange current density for H_2O/O_2 on the most effective OER catalyst in acid media (metallic iridium) was a factor of approximately 1,000 (Millet et al., 2011). These results explain why and how it is much easier to reduce noble metal contents for PEMEC cathodes than anodes.

$$\frac{i_o^{HER}}{i_o^{OER}} \approx 10^3 \quad (2.2)$$

Rozain and Millet (2014) outlined these findings such that the exchange current density for HER on platinum and the OER on iridium in acidic media are 10^{-3} Acm^{-2} and 10^{-6} Acm^{-2} respectively (Rozain and Millet, 2014), which are both considered to be the most attractive pure metal electrocatalysts respectively (Shiva Kumar and Himabindu, 2019). The exchange current density can be used to analytically model the activation resistance and double layer capacitance for the corresponding electrocatalyst material and electrolyte.

2.4.1 OER Electrocatalysts

Fabbri et al. (2014) examined the various reaction mechanisms of the OER reaction steps and outlined the potential-determining step (PDS), which involved the adsorption of O* species for the peroxide formation and subsequent proton release step (Fabbri et al., 2014), indicated by Equation (2.5). below. These findings are in line with others (Fang and Liu, 2010; Rossmeisl et al., 2007). The PDS is referred as the intermediate reaction that exhibits the poorest kinetics, such that it is this step that corresponds to majority of the entire reaction potential. For the most part, the materials that demonstrate lower overpotentials and therefore better reaction kinetics are well known and previous well studied noble metals.

Table 2.2: OER reaction steps for proton exchange electrolysis known as Krasil'shchikov path (Hansen et al., 2010).

Step 1	$H_2O_{(l)} \leftrightarrow HO^* + H^+ + e^-$	(2.3)
Step 2	$HO^* \leftrightarrow O^* + H^+ + e^-$	(2.4)
Step 3	$O^* + H_2O_{(l)} \leftrightarrow HOO^* + H^+ + e^-$	(2.5)
Step 4	$HOO^* \leftrightarrow O_{2(g)} + H^+ + e^-$	(2.6)

More specifically , these noble metals are most commonly rutile-type noble metal oxides are the standard for PEM OER catalysts such as rutile-type iridium oxide (IrO₂) and rutile-type ruthenium oxide (RuO₂) as they are superior at facilitating the PDS of the OER (Marshall et al., 2005; Rozain et al., 2016a). The same group took their research further by

identifying the binding strengths of RuO₂ and IrO₂ with the O* species. Turns out RuO₂ binds with the oxygen species too weakly and IrO₂ binds too strongly with respect to their respective theoretical activity. Rossmeisl et al. closely studied this phenomenon and mapped out the respective Gibbs free energy for each of the four-reaction steps on the volcano plot for IrO₂ and RuO₂, respectively, which clearly illustrates the difference in binding energy (Rossmeisl et al., 2007). Kotz et al. determined an optimal trade-off between stability and activity for a bimetal sputtered ruthenium and iridium oxide electrocatalyst, Ru_xIr_{1-x}O₂, which ranges between 0.5 < x < 0.8 (K&z and Stuck1, n.d.). Combining the two elements were deemed appropriate since RuO₂ has the lowest over potential of any pure material, however it suffers from stability, such that IrO₂ demonstrates a slightly larger overpotential with better stability (Carmo et al., 2013). Although, it is common to see rutile iridium without any ruthenium as the anode electrocatalyst due to the increased relative stability (Karimi and Peppley, 2017).

Unfortunately, these materials are very rare in terms of abundance and therefore are very expensive, as shown in Figure 2.4.2. Conversely, gold and platinum are 40 times and 10 times more abundant than iridium, receptivity (Carmo et al., 2013). In early 2012, iridium costed \$1,085 USD/troy ounce, whereas today, it costs roughly \$5,100 USD/troy ounce. As such, much of the recent research efforts have been aimed at increasing the amount of noble metal material used on a surface area per mass basis to ultimately reduce the capital cost and maintain performance. Moreover, research has been concentrated on the OER electrocatalyst due to the contributing relative sluggish kinetics and high capital cost relative to platinum for HER.

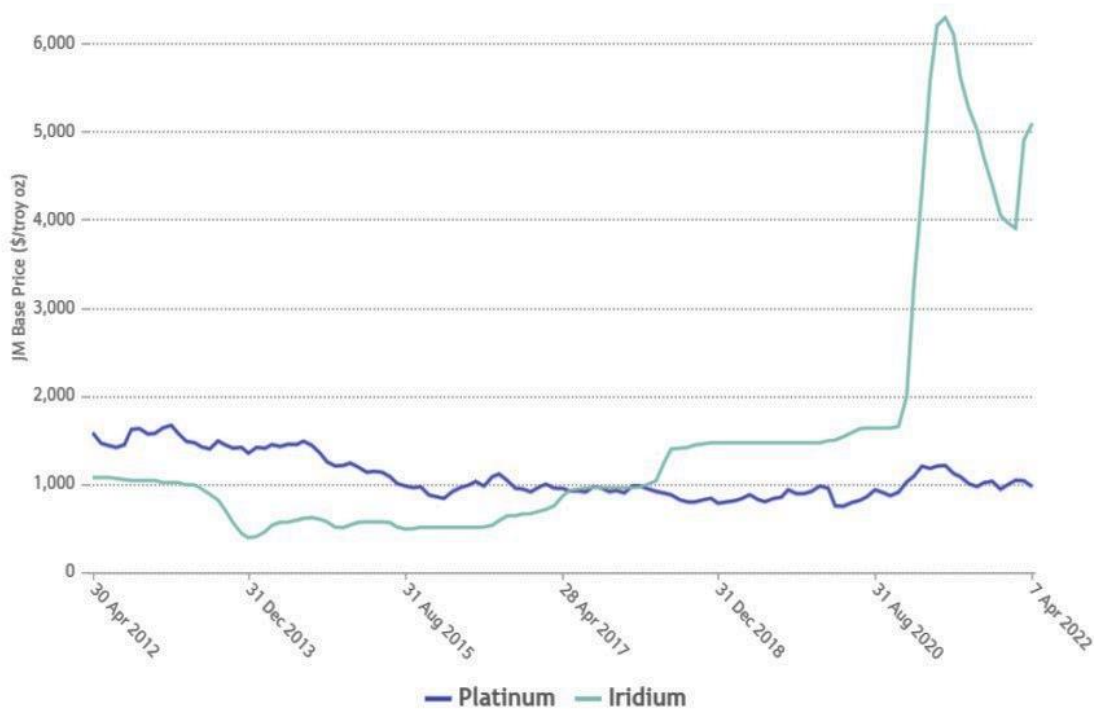
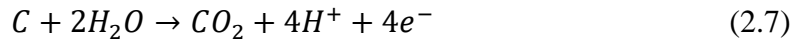


Figure 2.4.2: Price chart for platinum (HER) and iridium (OER) (Johnson Matthey, 2022).

One method to reduce the noble metal material used is to use an electrocatalyst support. Karimi and Peppley (2017) outlined that an effective OER support must exhibit appropriate specific surface area to reduce electrocatalyst agglomeration, high acidic corrosion resistance, and stability under high voltages (Karimi and Peppley, 2017). Mazúr et al. reported the unimportance of introducing an electronically conductive support since IrO_2 contributes sufficient conductivity (Mazúr et al., 2012), such that even non-conductive materials may be considered. The most common support material for electrocatalysts due to easy accessibility is carbon. However, carbon-supported electrodes that receive voltages exceeding 0.9V undergo breakdown in water environments (Rozain et al., 2016b). This phenomena forbids carbon as an anode support.



‘Valve metals’, which are characterized by materials with a high degree of thermodynamic instability such that they in turn readily adopt a passivation oxide (hydroxide) layer under the presence of O₂ and/or H₂O (Bystron et al., 2018). These materials in turn, once their thin passivation layer is formed, offer very high stability. Rutile titanium (TiO₂), rutile-type tantalum (TaO₂), tantalum pentoxide (Ta₂O₅), rutile-type tin (SnO₂), and rutile-type manganese (MnO₂), rutile-type molybdenum (MoO₂) are common valve metal supports, such that TiO₂ has the highest performance as it offers similar grain characteristics and size distribution homogeneity to IrO₂ (Mazúr et al., 2012). However, drawbacks are associated with the development of these passivation layers, which contribute to increased contact resistances.

Mazur et al. (2012) tested different TiO₂ supports that offered different specific surface areas to accommodate the ideal coverage compatibility with the IrO₂ catalyst (Mazúr et al., 2012). They discovered that the lowest specific surface area TiO₂ sample, of 10 m²/g, delivered to lowest Tafel slope with respect to the non-supported IrO₂ sample and the other TiO₂ samples of 50 and 90 m²/g, respectively. However, as a result of the hydroxide passivation layer, Lv et al. indicated bare TiO₂ is deemed as an unsuitable support due to poor electronic conductivity (Lv et al., 2019). This contradicts Mazúr et al. whom indicated the unimportance of a conductive support since the IrO₂ provides sufficient conductivity,

but rather emphasized the importance of stability and specific surface area (Mazúr et al., 2012).

Lv et al. (2019) studied the effect of introducing tungsten into the TiO_2 support to increase the electronic conductivity and stability alongside IrO_2 as the electrocatalyst (Lv et al., 2019). They found that heat annealed $\text{Ti}_{0.9}\text{W}_{0.1}\text{O}_2$ offered the best specific surface area and electronic conductivity to accommodate IrO_2 . Their support demonstrated a 39% voltametric charge increase relative to pure IrO_2 . Kadakia et al. (2012) studied the effect of introducing different amounts of tin and niobium, such that a composition of $(\text{Ir}_{0.4}\text{Sn}_{0.3}\text{Nb}_{0.3})\text{O}_2$ demonstrated similar results to pure IrO_2 (Kadakia et al., 2012). This represents a reduction of 60 mol.% of iridium loading with the tin and niobium mixture. Furthermore, all these results were studied with a 0.3 mg/cm^2 loading of $(\text{Ir}_{1-2x}\text{Sn}_x\text{Nb}_x)\text{O}_2$ composition on titanium foil GDL. Xu et al. (2012) considered different ratios of IrO_2 on a SnO_2 support, such that $\text{IrO}_2/\text{SnO}_2$ (2:1) demonstrated 1.7 V and 2 A/cm^2 with a noble-metal loading of 1.2 mg/cm^2 for anode and cathode respectively (Xu et al., 2012). They also determined that the SnO_2 support promoted the dispersion of IrO_2 nanoparticles and effectively removed adsorbed hydroxy species to promote reaction sites. de Pauli and Trassati outlined the surface enrichment effect of IrO_2 with SnO_2 (de Pauli and Trassati, n.d.), which validates the findings of Xu et al. above. Furthermore, they outlined the same PDS that Fabbri et al. discussed, which considers the binding strength of O^* species for the oxidation of HOO^* species (Fabbri et al., 2014). Ayers et al. compared a pure IrO_x catalyst, and IrO_x on SnO_2 and ITO (indium tin oxide), such that the pure IrO_x catalyst demonstrated the highest performance (Ayers et al., 2016). Moreover, the results that they

presented considered ultra-low loadings, 0.1-0.3 mg/cm², via core-shell and reactive spray deposition (RSD) techniques, an alternative to conventional catalyst coating methods (CCM). Karimi and Peppley studied IrO₂ with a TaC, WC, TiC, NbC, NbO₂, and Sb₂O₅-SnO₂ (ATO) support and found that the supports with less conductivity on their own demonstrated better performance than the other supports once iridium was introduced (Karimi and Peppley, 2017). Their results concluded Ir/ATO performed best, among the supports tested, such that ATO had a relatively large specific surface area of 35 m²/g and low conductivity of 0.01 S/cm.

2.4.2 HER Electrocatalyst

Regarding the cathode electrocatalyst for the HER, few papers discuss breakthroughs for these electrode materials since the kinetics for the OER are much more sluggish than the HER. Similar to the OER, the goal for improving HER electrocatalysts also involve reducing the usage of transition noble metals, primarily platinum for HER (Carmo et al., 2013). Millet et al. considered a carbon-supported cobalt clathrochelate instead of platinum, which demonstrated a 60% equivalent charge density of the conventional platinum HER electrocatalyst (Millet et al., 2011). Corrales-Sánchez et al. studied different combinations of two different MoS₂-based HER catalysts (Corrales-Sánchez et al., 2014). These included four different physical mixtures of MoS₂ and carbon black and two different MoS₂ nanoparticle loadings on a reduced graphene oxide. The results concluded that a 47 wt.% of MoS₂ on carbon black exhibited the best performance, however still not as good as platinum on carbon black. Hinnemann et al. applied density functional theory

(DFT) to calculate the free energy of atomic hydrogen bonding to different catalyst materials (Hinnemann et al., 2005), such that pure Ni and Mo bond too strongly, Au bonds too weakly, and Pt and MoS₂ exhibit relatively good bonding strengths to hydrogen, respectively.

Considering the minimal research effort towards non-platinum HER electrocatalysts relative to OER electrocatalyst, platinum supported on carbon is widely executed (Sapountzi et al., 2017; Wang et al., 2014). Due to the high roughness factor and low intrinsic overpotential of Pt/C catalysts, they pose minimal concern in terms of stability even at high current densities (Papakonstantinou et al., 2020).

2.4.3 Membrane

The main appeal surrounding the PEMEC considers the benefits that come with a highly conductive and selective proton exchange membrane, which ultimately delivers high purity hydrogen and oxygen gas with relatively low electricity consumption (Shiva Kumar & Himabindu, 2019). This technology was introduced in the late sixties due to the market production of Nafion®, which is a chemically stable sulfonated tetrafluoroethylene (TFE) based fluoropolymer-copolymer (Grigoriev et al., 2011). The material is widely referred as the first of its class of synthetic polymers called ionomers, which are polymer chains that exhibit ionic properties (i.e. ion conductivity). The ceramic membrane backbone is generated by the copolymerization of a perfluorinated vinyl ether comonomer with TFE (Mauritz & Moore, 2004). The perfluorinated membrane is submerged in sulfonic acid

thereby coating the channels with SO_3^- groups to facilitate intercluster transfer of cations and ion conductivity resulting in the formation of perfluorosulfonic acid (PFSA) (Grigoriev et al., 2011). More simply put, PEMs are ultimately strong acids in the solid form (i.e. PFSA), permitting the facile exchange of protons due to the high proton charge carrier density.

Xu and Scott (2010) noted that there are predominantly two ways to fabricate the membrane electrode assembly (MEA) for PEMEC, which include the catalyst coated GDL (CCG) and catalyst coated membrane (CCM) method (Xu and Scott, 2010). The first, CCG, involves spraying the catalyst onto the two respective GDLs, followed by sandwiching the two surfaces on either side of the membrane. The second, CCM, involves spraying, brushing, or blade coating catalyst onto the membrane (Carmo et al., 2013). In recent years, the CCM method has become the norm due to the enhanced interfacial characteristics and binding between the membrane and catalyst (Babic et al., 2017; Kumar and Himabindu, 2019; Thanasilp and Hunsom, 2010). Furthermore, the CCM method also permits the inclusion of introducing alternating layers of additional ionomer solution and catalyst slurry onto the membrane directly. Introducing ionomer solution into the catalyst layers increases the proton conductivity throughout the catalyst matrix and performs as a binder to provide three-dimensional structural support, and acts as a hydrophilic agent to support water transport to the catalyst interface (Xu and Scott, 2010). However, drawbacks associated with CCM include membrane swelling, wrinkling and/or cracking during fabrication (Thanasilp and Hunsom, 2010). This was concluded to be a consequence of the

isopropyl alcohol as the primary liquid media to makeup the catalyst slurry and ethylene glycol as the active additive.

Thanasilp and Hunsom (2010) studied the electrochemical performance of the decal-transfer CCM (CCM-DT) method in a fuel cell application (Thanasilp and Hunsom, 2010), such that it outperformed the conventional direct-wet-spray CCM (CCM-DS), which is the common fabrication method outlined above (i.e. CCM). Moreover, Ayers et al. identified that catalyst costs remain a major roadblock in terms of upfront capital necessary for scaling up these electrochemical systems and tested the state-of-the-art combination of core-shell catalysts and advanced manufacturing processes (Ayers et al., 2016). They demonstrated that their method performed better against other conventional PEM MEAs, with a noble metal loading of 0.1 mg/cm^2 for both Pt and Ir. Furthermore, they compared their MEA with other reported deposition conditions, such that their MEA was one of the best performing low noble-metal MEAs to date. Even more promising, they demonstrated stable-steady-state performance at 2 A/cm^2 and 50°C for 600 hours.

There are many different types of Nafion® ionomers commercially available, such that they follow a unified naming designation relating the ion conductivity and thickness. For example, Nafion® 117, refers to an equivalent weight (EW) of 1100 g/eq and nominal thickness of 0.007 in., such that the EW is the number of grams of dry Nafion® per mole of sulfonic acid groups when the material is in the acid form (Mauritz and Moore, 2004). The lower the EW corresponds to better performance, indicated by a higher concentration of sulfonic groups, which assist ion conductivity. These polymers have become recently

termed as long-sidechain (LSC) PFSA, ever since the discovery of the smaller short-side chain (SSC) PFSA, called Aquivion®. Siracusano et al. (2014) determined that Aquivion® outperformed Nafion®, more specifically E87-12S and N115, respectively, in terms of delivering a lower ohmic/series resistance, polarization resistance, and charge transfer resistance, indicating a better electrolyte (i.e. membrane) to electrocatalyst interface (Siracusano, 2014). They attributed the lower polarization resistance to a better triple-phase boundary as a consequence of the SSC structure, allowing for a lower EW (i.e. higher specific density of sulfonic acid groups). Their performance results for Aquivion® were 1.8V at 3.2 A/cm² in 90°C with an IrO₂ and Pt/C electrocatalyst. The naming of E87-12S corresponds to an EW of 870 g/eq and thickness of 120 µm. Furthermore, the Aquivion® ionomer is characterized by having both a higher glass transition temperature and higher crystallinity, thereby improving thermal stability and reducing gas crossover (Siracusano et al., 2017). Further testing is recommended as Nafion® seems to be the standard (al Shakhshir et al., 2017; Rozain et al., 2016b; Siracusano et al., 2017), while recent findings suggest that there pose better options. Other PFSA membranes that are commercially available include Fumapen®, Flemion® and Aciplex® (Kumar and Himabindu, 2019).

Alternatively, hydrocarbon based non-fluorinated membranes also present opportunity, in terms of cost significant reduction and simplification concerning end-life disposal due to the avoidance of fluorine usage (Wei et al., 2010). The current price for bare polysulfone polymer is about \$10/kg and adding the cost of sulfonation and casting/extrusion towards fabricating the final polysulfone membrane is still much cheaper than Nafion®, which

costs roughly \$5000/kg (Siracusano et al., 2014). These materials consist of an organic-chain backbone, such that, similarly to TFE, sulfonic functional groups are introduced to provide the polymer with ion conductivity traits (Schalenbach et al., 2013). Among the long list, the more promising non-fluorinated polymers that can withstand PEMEC temperatures and are susceptible to sulfonation (i.e. acceptance of sulfonic acid to evolve into an ionomer like material), include polysulfones, polybenzimidazoles, polyetherketones, and poly(aryl ether sulfones) (Siracusano et al., 2013; Wei et al., 2010). Siracusano et al. (2013) compared the performance of Nafion® 115 and sulfonated polysulfone (SPSf) membranes in terms of gas-crossover, proton conductivity and electrochemical performance (Siracusano et al., 2013). The Nafion® slightly outperformed the SPSf, such that at 1.8V the current draw was 1.29 and 1.08 A/cm², respectively. Schalenbach et al. (2013) noted that these membranes are favourable for high pressure operation due to their reduced gas permeability (Schalenbach et al., 2013).

Another membrane that was considered specifically for fuel cell application, was the commercial AB-PBI membrane from Fuma-Tech (Unnikrishnan et al., 2019). The research conducted with this membrane tested under temperatures up to 160°C which serves to demonstrate potential for high pressure and high temperature membrane application. Ginner Electrochemical Systems (GES) developed a dimensionally stable membrane (DSM) for high pressure and temperature electrolysis application by spraying multiple thin coats of liquid Nafion® solution onto a Kapton® support (i.e. high-strength polyimide material) (Cropley and Norman, n.d.). The Young's modulus of Kapton® is 2,900 MPa, which is exceptionally stronger than wet Nafion® 112 of 70 MPa.

As aforementioned, a PEMEC can operate at high pressures due to the presence of the membrane which for the most part, only permits hydrogen ion transport, and has a relatively high tensile strength to accommodate the pressure build-up between the two electrode chambers during differential pressure operation. As a result, a PEMEC can produce high pressure hydrogen in a one-step process, thereby removing the energy consumption necessary to mechanically compress the gas for storage and/or transportation. Onda et al. (2004) and Todd et al. (2014) analytically modelled high pressure electrolysis and compared the total energy consumption with low pressure electrolysis paired with mechanical gas compression, such that the latter consumed 5% more energy (Onda et al., 2004; Todd et al., 2014).

Much research has been focused on membrane properties to ensure minimal gas-crossover and electro-osmotic drag of water during high pressure operation (Grigoriev et al., 2009). Gas contamination can raise concerns, in terms of efficiency losses, but also in terms of safety due to hydrogen's ability to spontaneously oxidize with oxygen (lower explosive limit 4 mol.% H₂ in O₂) (Schalenbach et al., 2013). Furthermore, hydrogen recombination with oxygen inside the membrane can also be detrimental due to the heat produced, causing local delamination in the membrane.

The main characteristics that consider reducing the transport of undesired contents through the membrane involve changing the membrane thickness, modifying the membrane properties, adding a composite to the membrane, and altering the operating conditions of

the cell. Additionally, external gas recombiners can be installed to promote H₂/O₂ recombination within the separated gas chambers, thereby reducing contamination and maintaining safety (Grigoriev et al., 2011). This option should be considered only as a backup safety mechanism as the efficiency losses due to undesired transport of contents through the membrane are not resolved.

A demonstrated additional benefit of high-pressure operation includes the reduction towards ohmic resistances due to oxygen and hydrogen gas bubbles that form on the surface of electrodes and transport through the GDL (Fabbri et al., 2014). This phenomenon is due to the reduced electrode surface area that bubble formation infringes on the electrodes, allowing for an increased electrode-electrolyte surface area interface. Therefore, high current densities are more favourable during high pressure operation due to the improved mass transport of the gaseous production away from interfaces.

Concerns arise if current collectors are pressed too firmly against each other, thereby compressing the MEA which sits in between the current collectors. Excessive force can cause the catalytic layer to be locally crushed and even destroyed leading to reduced lifetime and efficiency of the MEA (Millet et al., 2011). Operating at elevated pressure has the same effect on the membrane as applying clamping pressure on the current collectors. This excessive crushing force reduces the internal channels for cation migration. However, as indicated in the same study, firmly pressing the two current collectors together is necessary for appropriate electrical contacts and transport media between the various MEA layers, indicated in Figure 2.4.1, reducing the ohmic and activation resistances. With

respect to further reducing activation resistances concerning electrochemical interface performance, operating under high-current densities is shown to be effective due to the high abundance of electrons present. This trade-off should be closely considered, since for the most part, operating at high-current densities accompany increased ohmic resistances (Schalenbach et al., 2013), contributing to a larger the total resistance, increasing the cell potential. The result is (derived from Equation (3.17) in Chapter 3):

$$E_{cell} = E_0 + \frac{RT}{2F} \ln \left(\frac{\sqrt{P_{O_2}} P_{H_2}}{P_{H_2O}} \right) + iR_{total} \quad (2.8)$$

2.4.4 Gas Diffusion Layer

The gas diffusion layer (GDL) permits the transport of reactants and products to and from the bulk and electrocatalyst interface and offers the necessary thermal and electrical conductivity for electron transport. GDL characteristics also include necessary material structure compatibility with the catalyst for effective contact, and proficient stability for operating in corrosive environments (Babic et al., 2017). Carbon-based nanofibers or clothes are frequently used as catalyst support GDLs due to their high surface area and conductivity, however as aforementioned, carbon cannot be present in the anode due to the applied voltages, causing the carbon to oxidize (Babic et al., 2017). Titanium, or commonly rutile titanium, is often the chosen anode GDL material due the corresponding high stability characteristics and similar bond structure of rutile-type iridium (Bystron et al., 2018). The titanium anode and carbon cathode GDL are selected for the same reasons stated above, in Sections 2.4.1 and 2.4.2, concerning appropriate catalyst supports for OER and HER,

respectively. Al Shakhshir et al. (2017), Rozain et al. (2016), and Siracusano et al. (2012) and many others used a titanium felt and carbon cloth for the anode and cathode GDL for catalyst backing, respectively (Al Shakhshir et al., 2017; Rozain et al., 2016; Siracusano et al., 2012). Titanium grids (Siracusano et al., 2012) and titanium cloth (Al Shakhshir et al., 2017) manufactured by Franco Corradi, and sintered fibrous titanium by Sylatech Analysetechnik (Papakonstantinou et al., 2020) have also been used. In terms of chemically treating the materials, more specifically the treating of the titanium to deal with passivation layer growth, details are discussed in Section 4.2.

In terms of electrically connecting the two GDLs to and from the power source, which are responsible for charging the two electrocatalysts, certain considerations are involved due to the high acidity and oxidating conditions on the anode side. The high acidic environment remains concentrated at the anode interface and is less severe further from the electrocatalyst interface. As a result of the relative lesser acidic conditions on the opposite side of the GDL, to the electrocatalyst, stainless steel plates are commonly used due to high electrical conductivity and relatively high corrosion resistance (Siracusano et al., 2012; Wei et al., 2010). These plates are typically referred to as either current collectors, porous current collectors (PCC) or bi-polar plates for multi-cell electrolyzers. Other researchers used sintered titanium plates to connect the electrically connect the GDL to the circuit wiring (Grigoriev et al., 2014; Rakousky et al., 2017). Similar to the drawbacks associated with passivation layer growth concerning the titanium anode support, a platinum coating is introduced to the sintered titanium current collector for long-term stability (Grigoriev et al., 2009).

2.4.5 Degradation

To effectively maximize the high upfront investment costs associated with the electrocatalysts, membrane, and porous diffusion layer, enhancing their respective durability is paramount to ultimately delay their replacement. Efforts have been spent to identify degradation mechanisms for the respective materials, their interplay, and their sensitivity to specific operating conditions. Mechanisms that are considered as degradation are identified as either chemical, thermal or mechanical which influence the electrochemical performance over time during prolonged operation. These changes will affect the voltage demand (i.e. voltage increase to maintain constant production rate and therefore constant current), due to the gradual evolution of higher irreversible impedance sources, thereby increasing the operating costs of increasing electricity consumption over time. Understanding these phenomena are critical to manage the upfront capital and operating costs by ultimately maintaining or improving the cell's endurance characteristics. Chemical degradation is assigned to any disadvantageous changes within the membrane, electrocatalyst, conducting ionomer in the electrocatalyst and/or GDL due to undesired gas or ion diffusion. This is a very broad class of degradation in terms of underlying triggers, such that only the more common ones will be discussed. At the top of the list, hydrogen and oxygen can migrate through the membrane due to diffusion, pressure, and/or electro-osmotic drag (Schalenbach et al., 2013). The transport of the two gases through the membrane pose not only safety concerns (Grigoriev et al., 2009), and reduced efficiencies, but also are prone to recombine to form H_2O_2 at the cathode (Papakonstantinou et al.,

2020). The H_2O_2 can combine with cation impurities, mainly from stainless steel components, that will decompose to form reactive radicals that threaten the MEA. For a fuel cell application, the radicals produced from the Fenton reaction caused a sudden cell death when 5ppm of Fe^{3+} ions were present (Li et al., 2020). The same group also indicated that Cu^{2+} can help to catalyze the Fenton reaction, thus assisting degradation (Li et al., 2020). Furthermore, Li et al. (2019) indicated that Al^{3+} , Fe^{3+} , Cr^{3+} , Ni^{2+} , and Mg^{2+} have a stronger affinity towards the sulfonic acid groups than H^+ protons (Li et al., 2019). These impurities then block the active channels within the membrane at the interface, thus reducing the proton conductivity in the membrane. Banas et al. (2018) determined that Ca^{2+} caused uniform thinning of the CCM of a PEM fuel cell, such that the platinum loadings on both the anode and cathode were unchanged, indicating that the carbon support was shedding (Banas et al., 2018). Furthermore, Ca^{2+} has been identified to congregate by forming hydroxide precipitates between the cathode and membrane interfaces, thus blocking active cathode sites (Grigoriev et al., 2014). Fortunately, much of these mechanisms can be significantly avoided if the feed water is circulated periodically through a deionizing process.

Thermal degradation includes operating the cell at temperatures such that materials, mostly concerning the membrane, become unstable. These instabilities consider worst case of membrane bubbling and delamination but also increased rates of product gas crossover (Buttler and Spliethoff, 2018; Grigoriev et al., 2009).

Mechanical degradation can arise due to the heterogenous makeup of different materials that comprise the MEA. Uneven stresses due to rapid temperature or pressure change can cause material separation, resulting in major performance reduction or MEA failure (Papakonstantinou et al., 2020). As well, mechanical damage can also include membrane cracking, tearing, pin holing, and physical punctures.

Rakousky et al. (2017) tested the effect of different current profiles on the long-term PEMEC performance (1,009 hours), with an IrO₂/TiO₂ anode and Pt/C cathode (Rakousky et al., 2017). For a steady state of 1 A/cm², no degradation was observed. The other tests, which involved a steady 2 A/cm² and continuously intermittent supply of 2 to 1 and 2 to 0 A/cm², all showed signs of performance degradation. Of these, the steady 2 A/cm² showed the least degradation resistance with a corresponding voltage drift of 196 μV/h. They reported these changes due to increased ohmic resistance from gradual membrane diffusion deactivation and a decreasing anode exchange current density due to anode poisoning from titanium cations. More promisingly, Pt/C are reported to offer high stability, thereby not affecting the performance, even at high current densities due to the facile kinetics of the HER, which is indicated by the low intrinsic HER overpotential (Fabbri et al., 2014; Papakonstantinou et al., 2020). In summary, higher current densities will facilitate higher rates of gas production at the cost of higher degradation rates, which is congruent for all electrochemical systems (Siracusano et al., 2012).

Rozain et al. (2016a) studied the effect of two different current supply profiles, a uniformly stepped profile from 0.04 to 2 A/cm² at 0.2 A/cm² increments, and a real solar-type profile

based on solar radiation and cloud interference etc., on the electrochemical performance of three different MEA electrocatalyst (Rozain et al., 2016a). As well they considered different loadings of pure IrO₂ and 50 wt.% IrO₂/Ti, such that the latter demonstrated lower cell potentials and increased endurance characteristics, due to the increased IrO₂ dispersion of introducing titanium micro-sized particles into the IrO₂ catalyst layer. Even more interestingly, the highest performing IrO₂/Ti loading was the smallest loading, 0.12 mg/cm², which was attributed to reduced mass transport limitations and sufficient electronic conductivity through the catalyst layer. The pure IrO₂ samples suffered from a reducing electrical interface between the catalyst and titanium current collector due to the surface of the correct collector oxidizing. By adding the titanium microparticles into the catalyst matrix, the contact resistance at the interface reduced by activating more catalyst layers, thus permitting a lower cell voltage (less than 2V at 2 A/cm²) and leading to less titanium oxidation. Their degradation results were a very promising 27 and 2 μV/h at 1 A/cm² for the stepped and solar-type profiles, respectively.

Very promisingly, Lettenmeier et al. (2016) observed a negative degradation rate with an iridium black anode (Lettenmeier et al., 2016). This was attributed to the iridium black gradually oxidizing to form rutile iridium (IrO₂). Unfortunately, after time, iridium was found to leach onto the membrane, which potentially could cause cell failure.

As aforementioned, titanium is characterized as a valve metal, such that when exposed to oxygen or water, the outer surface passivates to form a TiO₂ layer, thereby protecting the material from further oxidation, however significantly reducing electrical conductivity in

non-/semiconducting manner. For this reason, Bystron et al. outlined and confirmed the effect of chemically etching titanium felt to not only remove the predisposed passivation layer present on titanium before electrolysis but also to reduce passivation growth that takes place during electrolysis (Bystron et al., 2018). Chemical treatment is also recommended by the manufacturer of the titanium felt for the same reasons stated. Treatment involves cleaning followed by submerging the titanium felt in a 35% HCl solution to saturate the metal with hydrogen, facilitating the formation of titanium hydrides within the bulk and on the metal surface. The post-treated materials considers the surface to be covered in titanium hydrides, thus removing and reducing future TiO₂ layer growth (Bystron et al., 2018).

Other methods of reducing degradation include externally coating the titanium with platinum (Grigoriev, Millet, Volobuev, et al., 2009) or gold (Rakousky et al., 2017). These coatings reduce titanium embrittlement although may suffer exfoliation with high current densities.

One group demonstrated that increasing the clamping pressure of the bipolar plates can extend the cell life by reducing undesired cross-over. This is because the rate of membrane degradation is related to the rate of undesired cross-over, such that cation sites become blocked (Li et al., 2019). Increased MEA clamping pressure causes the pore size of the membrane and GDL to be reduced, which reduces the transport of water and other impurities through the GDL which in turn reduces membrane degradation over time (Al Shakhshir et al., 2017). However, this reduction in transport of water and other impurities ultimately reduces the overall transport for all compounds including the accessibility of

water to reach reaction sites at the catalyst interface, thereby reducing the overall hydrogen ion transport. Alternatively, when the MEA is pressed too firmly, the catalytic layers can become crushed, reducing the lifetime and efficiency significantly (Carmo et al., 2013). Al Shakhshir et al. (2017) studied the electrochemical performance of applying two different clamping pressures onto the MEA, such that the 150-psi setup demonstrated lower charge transfer resistance, lower gas crossover, lower MEA capacitive impedance, and therefore lower degradation compared to the 60-psi setup (Al Shakhshir et al., 2017). Further testing is necessary to understand the effect of clamping pressure and the associated limitations with respect to cross permeation and cell integrity.

The simplest mitigation solution for reducing cross-permeation involves increasing the membrane thickness, however, at the expenditure of increasing the ohmic resistance (Grigoriev et al., 2009). In other words, increasing the membrane thickness can help prevent long-term degradation via cross-permeation suppression but with the increase of ohmic resistance. These were the same conclusions that Yuan et al. (2012) found, such that hydrogen crossover had the biggest impact on degradation (Yuan et al., 2012), causing further membrane thinning and pinhole formation. By reducing the cross-permeation of contaminants, the response is shown by a lesser membrane and electrocatalyst degradation rate however at a higher electricity consumption. Placca and Kouta (2011) performed a fault tree analysis for a proton exchange membrane fuel cell (PEMFC) to identify the most sensitive components to the overall degradation of the cell (Placca and Kouta, 2011). Further work should be done to study this relationship with the focus on PEMEC.

In addition to increased product gas crossover under higher current densities, higher proton transport also occurs, thereby increasing the concentration of proton ions at the interfaces, further contributing to increased corrosion rates for susceptible materials. Furthermore, bubble removal is shown to affect the mass transport of the reaction (Siracusano et al., 2012), and increasingly so under higher current densities. This affect is as issue for all conventional bi-directional electrochemical systems, thus contributing to increased ohmic resistances. Hodges et al. (2022) have proposed a new innovative uni-directional AEMEC system which negates the gas-liquid interference and therefore inefficiencies of bubble removal (Hodges et al., 2022), such that the reactants are capillary-action fed through the membrane, which introduces the possibility of implementing a similar design for PEMEC.

2.4.6 Hot-Pressing Assembly

It is common to hot-press the MEA, during fabrication, to effectively embed the catalyst layers onto membrane, to increase interface contact area and thus reduce ohmic resistances and reduce catalyst delamination (Nikiforov et al., 2016; Schalenbach et al., 2016; Shan et al., 2015). This process of hot-pressing, otherwise referred to as annealing or calcination, helps to promote good contact between the three-phase region, which considers the membrane, electrocatalyst and GDL layers. Liang et al. (2007) demonstrated that hot-pressing for 60-minute versus 3-minute improved durability, however had little performance change was present (Liang et al., 2007). Concerning the MEAs that Corrales-Sanchez et al. (2014) tested, hot-pressing demonstrated worse performances than the same MEA without hot-pressing preparation (Corrales-Sánchez et al., 2014). Reasons explaining

this phenomenon were left unknown, however should be noted that this experiment involved a MoS₂ catalyst on a reduced graphite support, instead of the conventional Ir-based anode.

2.5 Gaps in Literature

The number of scientific reports towards HER and OER have increased exponentially since 2010 (Kumar and Himabindu, 2019). It is clearly noticeable that hydrogen electrolysis research lags behind hydrogen fuel cell research due to the earlier demand for fuel cells for space shuttles. As a result, much of the commercially available membrane and catalyst materials and associated research findings are due to the development of fuel cells. Research in this area is likely to continue to occur due to the associated upsides towards achieving a so-called cleaner society assuming continued breakthroughs occur.

Many publications have considered PGM and non-PGM catalysts in supported and unsupported makeups, while also varying composition and loading amounts as outlined previously. Furthermore, steady-state, dynamic-state, and intermittent-solar-state have been tested to understand the associated degradation, dissolution, and membrane thinning rates. As well, cation impurities have also been considered to understand long-term performance hinderances on catalysts and membrane. However, many of these phenomena have been studied in strict isolation, calling for future studies to appropriately couple multiples of these characteristics to work towards an optimized setup.

One area that was difficult to find thorough investigations considered the process of MEA fabrication. Of these papers, they studies considered different annealing temperatures and durations, and fundamentally different coating methods such as direct-spray onto GDL, direct-spray onto membrane, decal-transfer, and more recent methods of co-crystallization or spray under irradiation (Spöri et al., 2017), however the description of their process of fabrication is limited making it difficult to build upon past experiments. The common overall goal that researches consider when evaluating these methods are loading (i.e. CAPEX) and stability (i.e. OPEX) relative to current density (i.e. gas yield) such that the fabrication method has a significant influence on economic competitiveness.

Chapter Three: Analytical Model

3.1 Models from Literature

The models that simulate electrolysis first consider the reversible open-circuit situation which is based on the Gibbs free energy change outlined by Equation (2.1) (Aubras et al., 2021; Marangio et al., 2009; Schalenbach et al., 2013). The next steps involve analytically describing the irreversible mechanisms at play, which are similar but vary slightly. The models are similar such that they attempt to relate the overpotential (i.e. irreversible voltage contribution) to MEA parameters such as the porosity, thickness, ionic and electric conductivity, gas solubility and permeability associated to the membrane and catalyst layers. They all however include and require fitting parameters from in-situ experiments to calibrate the equations accordingly.

3.2 Model Development

The overpotential and current density reported in the literature were then be used in conjunction with an analytical model based on electrochemical and thermodynamic principles to determine an up-to-date cost estimate of electrolysis in a high temperature environment. Mathematically, the electrolysis of water phenomenon can be modelled using the first and second law of thermodynamics which in the form of Gibbs free energy formula, given by:

$$\Delta H(T) = \Delta G(T) + T\Delta S(T) \quad (3.1)$$

where ΔH is the enthalpy change, ΔG is the Gibbs free energy change, T is the absolute temperature, and ΔS is the entropy change. The energy associated with the chemical conversion can be modelled using the first and second laws of thermodynamics, Equation (3.1). The enthalpy and entropy contribute towards the required amount of work that must be put into the system for a non-spontaneous reaction to progress. The enthalpy and entropy with respect to temperature were modeled using Kirchhoff's equations:

$$\Delta H(T) = \Delta H_{298.15}^{\circ} + \int_{298.15}^T \Delta C_p dT \quad (3.2)$$

$$\Delta S(T) = S_{298.15}^{\circ} + \int_{298.15}^T \frac{\Delta C_p}{T} dT \quad (3.3)$$

The values for specific heat capacity slightly vary between publications as their method of approximating were different. Listed below in Table 3.1, two different approximations from two different publications were used for heat capacity of the respective compounds involved in the reaction as a function of temperature.

Table 3.1: Heat capacity data for hydrogen, oxygen, and water.

Publications	Compound	Heat Capacity (C_p)(J/mol/K)	Sources
(Shin 2007)	(H ₂)	$27.28 + 0.00326T + 50000/T^2$	(JA., 1985)
	(O ₂)	$29.96 + 0.00418T - 167000/T^2$	(Perry RH, 1973)
	{H ₂ O}	75.44	
	(H ₂ O)	$30.00 + 0.01071T + 33000/T^2$	
(Mingyi 2008)	(H ₂)	$(29.07 - 0.836) \times 10^{-3}T + 20.1 \times 10^{-7}T^2$	(F. Xiancai, 2004)
	(O ₂)	$(25.72 + 12.98) \times 10^{-3}T - 38.6 \times 10^{-7}T^2$	
	{H ₂ O}	75.30	
	(H ₂ O)	$(30.36 + 9.61) \times 10^{-3}T + 11.8 \times 10^{-7}T^2$	

(); gas phase, { }; liquid phase.

Balta et al. (2016) used another approach to determine the enthalpy and entropy change at non-standard temperatures using the Shomate constants and corresponding Taylor series, shown in Equation (3.4) and Equation (3.5) (Balta et al., 2016). This approximation was sourced from the NIST (National Institute of Standards and Technology) for the application of modelling high temperature steam electrolysis.

$$h - h_0 \text{ (kJ/mol)} = At + B \frac{t^2}{2} + C \frac{t^3}{3} + D \frac{t^4}{4} - E \frac{1}{t} + F - H \quad (3.4)$$

$$s - s_0 \text{ (J/K/mol)} = A \ln(t) + Bt + C \frac{t^2}{2} + D \frac{t^3}{3} - E \frac{1}{2t^2} + G \quad (3.5)$$

where t is $T/(1000)$ and T is the temperature in Kelvin of the compound, and A, B, C, D, E, F, G and H are constants, listed in Table 3.2. Based on their results, this method provided results in line with the other two approximations listed in Table 3.1 above.

Table 3.2: Enthalpy of formation and Shomate constants.

Compound	(H ₂ O)	(O ₂)	(H ₂)
h_f° (kJ/mol)	-242	0	0
A	30.092	29.659	33.0661
B	6.83251	3.13726	-11.363
C	6.79344	-1.1865	11.4328
D	-2.5345	0.09578	-2.7729
E	0.08214	-0.2197	-0.1586
F	-250.88	-9.8614	-9.9808
G	223.397	237.948	172.708
H	-241.83	0	0

(); gas phase, { }; liquid phase.

The reversible amount of work applied is equal to the electric cell potential required to dissociate water into hydrogen and oxygen, at the system temperature, given by:

$$\Delta G(T) = nFE_{cell}(T) \quad (3.6)$$

This equation utilizes Faraday's constant, F , which relates the number of charges passed per mole of a full cell reaction. The total amount of thermal energy consumed to split water can be considered as the entropy change, ΔS , for a given temperature, T (Sigurvinsson et al., 2006). However, the enthalpy change, entropy change, and Gibbs free energy for this conversion depend on temperature, as shown in Equation (3.1). The total enthalpy increases slightly versus temperature, whereas the entropy change, and Gibbs free energy significantly increase and decrease, respectively, with temperature increase.

To clarify, the sum of the enthalpy and entropy change between the products and reactants at a given temperature of the reaction is equal to the Gibbs free energy, given by Equation (3.1), which corresponds to the reversible work for the reaction at that temperature. Applying Equation (3.6), the electrochemical voltage required (i.e. reversible cell potential) to make the reaction proceed can be determined for that operating temperature.

$$\begin{aligned}
 E_{cell} &= \frac{\left(\Delta H_{298.15, H_2}^\circ + \int_{298.15}^T \Delta C_{p, H_2} dT - T \left(S_{298.15, H_2}^\circ + \int_{298.15}^T \frac{\Delta C_{p, H_2}}{T} dT \right) \right)}{nF} \\
 &+ \frac{\frac{1}{2} \left(\Delta H_{298.15, O_2}^\circ + \int_{298.15}^T \Delta C_{p, O_2} dT - T \left(S_{298.15, O_2}^\circ + \int_{298.15}^T \frac{\Delta C_{p, O_2}}{T} dT \right) \right)}{nF} \quad (3.7) \\
 &- \frac{\left(\Delta H_{298.15, H_2O}^\circ - 298K(S_{298.15, H_2O}^\circ) \right)}{nF}
 \end{aligned}$$

Although, Equation (3.7) does not account for pressure changes since the correlations used from literature to obtain the heat capacity of the respective species only consider temperature. Figure 3.2.1 displays the various components of Equation (3.7) as a function of temperature. Todd et al. (2014) analytically modelled temperature and pressure effectively by employing equations-of-state (EOS) from thermodynamic properties (Todd et al., 2014).

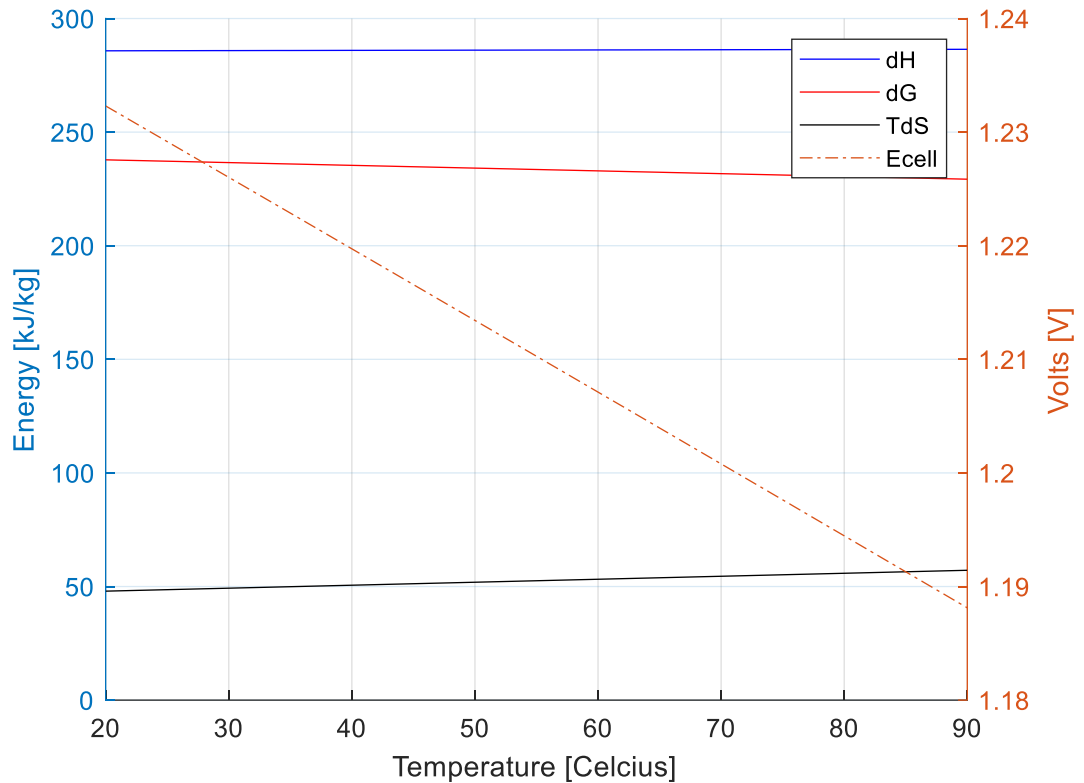


Figure 3.2.1: Energy demand for HTSE as a function of temperature. As the temperature rises, the amount of electricity required to produce a unit of hydrogen is reduced shown by the dotted line, E (reversible cell potential).

The intention of pursuing electrolysis under high pressure is introduced once considering the storage and transportation of hydrogen, which considers the energy density. Hydrogen at room temperature and atmospheric pressure has a density of 0.1 kg/m^3 approximately. If hydrogen is compressed to 35 MPa and stored at room temperature, the density increases to roughly 23 kg/m^3 , such that the energy density increases accordingly as well. To do this compression, the hydrogen production via electrolysis typically involves post-electrolysis mechanical compression, requiring energy input to run compressors. Awashi et al. (2011) concluded that increasing the operating pressure of the electrolysis cell leads to a decrease

in cell performance due to the resulting partial pressure increase of the species, demonstrated by Equation (3.12), the Nernst Equation (Awasthi et al., 2011). More promising however, recent reports analyzed the thermodynamic and mechanical work between the energy inputs for mechanically compressing the hydrogen versus performing high pressure electrolysis. The reports analytically proved that electrolysis under pressure consumes approximately 5% less total energy than low pressure electrolysis paired with post mechanical compression (Onda et al., 2004; Todd et al., 2014). Moreover, operating at increased pressures allows water to stay liquid at temperatures above 100°C thereby further assisting the potential for thermodynamic gains while performing liquid water electrolysis at temperatures excess of 100°C. For this reason, ensuring high-temperature and high-pressure operation for electrolysis is necessary to facilitate the best opportunity for electrolysis to be competitive.

The Nernst equation can approximate the reversible cell potential under non-standard temperature and pressure (STP) conditions, to understand how temperature and pressure influences the total energy input of consumed electricity. Under non-standard conditions, particles will experience short-range forces/crowding and will ultimately contribute to entropy and enthalpy corrections. These corrections can be accounted for using a dimensionless parameter, called the activity, a , to relate the short-range forces/crowding in terms of concentration, c , molality, m , available sites, x , or partial pressure, p . The quantities are typically scaled such that the activity coefficient, γ , is unity for the standard state of a single species. Error is derived with this assumption as the activity coefficient is

never truly unity. This assumption, $\gamma = 1$, is acceptable for ion concentrations below 0.001 M since the concentration or partial pressure etc. become the independent variable.

$$a_i = \gamma_i c_i = \gamma_i m_i = \gamma_i x_i = \gamma_i p_i \quad (3.8)$$

The Nernst equations model each half-cell reaction separately. This permits the calculation of the reversible electrochemical cell potential under non-STP conditions. The equations are calibrated using the standard cell potentials, E_0 , for each respective half-cell reaction. Standard cell potentials are experimental based measurements for many common half-cell reactions under STP conditions and are found in many published textbooks.

$$E^{anode} = E_0^{anode} + \frac{RT}{nF} \ln \left(\frac{a_{products}}{a_{reactants}} \right) \quad (3.9)$$

$$E^{cathode} = E_0^{cathode} + \frac{RT}{nF} \ln \left(\frac{a_{products}}{a_{reactants}} \right) \quad (3.10)$$

Cumulatively, the Nernst half-cell equations for the respective anode and cathode reactions can be added to produce the reversible full-cell electrochemical potential, E_{cell} .

$$E_{cell} = E^{anode} + E^{cathode} \quad (3.11)$$

Presenting the activity coefficients in terms of partial pressures, the Nernst equation for electrolysis of water is as follows.

$$E_{cell} = E_0 + \frac{RT}{2F} \ln \left(\frac{\sqrt{P_{O_2}} P_{H_2}}{P_{H_2O}} \right) \quad (3.12)$$

Schalenbach et al. (2013) and Marangio et al. (2009) verified that this expression agrees with in-situ electrochemical experimental results, such that increasing the pressure of produced gas will in turn increase the reversible cell potential (Marangio et al., 2009; Schalenbach et al., 2013). Millet et al. (2011) approximated the negative effect on the thermodynamic voltage of increasing operating pressure to be +10mV/decade of pressure, however, they also indicated that the efficiency of the cell increases with increasing pressure, even more so under higher current densities (Millet et al., 2011). Babic et al. (2017) assumed the solubility of H₂ and O₂ in water behave as ideal gases up to 100 bar, such that at 60°C, the Nernst potential increases approximately 33mV and 50mV per decade of pressure for differential and balanced pressure operation, respectively (Babic et al., 2017). Differential operation considers the oxygen side to remain at atmospheric pressure whereas balanced operation considers both hydrogen and oxygen sides operate at equal pressure.

To effectively compare high-pressure electrolysis to atmospheric-pressure electrolysis with post-mechanical compression, the actual operating potential (i.e. irreversible cell potential) must be considered. Unfortunately, actual test results that would correspond to high pressure irreversible potentials were not gathered in this work due to the inability of the built electrolysis cell to contain the produced gases without leakage. The irreversible cell

potential can be used to effectively compare material components and cell configuration since these factors affect the electrical, ionic, polarization and activation resistances. Figure 3.2.2 illustrates a theoretically simplified equivalent electrical circuit of an electrolysis cell, which relates the various mechanisms that contribute to the irreversible losses.

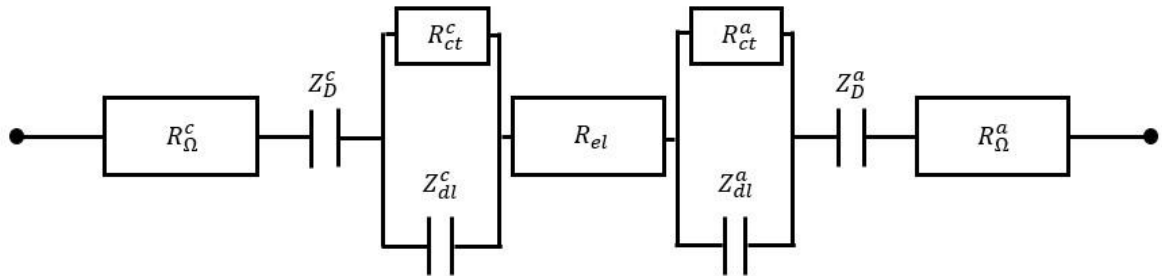


Figure 3.2.2: Equivalent circuit for internal impedances of electrolysis cell.

Instead of breaking down the cell into equivalent impedances, which equate to a voltage drop characterized by overpotential when current is passed through the cell, the cell can be broken down directly into various sources of overpotential as functions of current. This permits the equivalent impedances and Nernst Equation to model the irreversible potential. R_{Ω} is the ohmic resistance, for the cathode and anode, which is the contribution of electrical resistance from metallic cell components for conducting electricity, and the ionic resistance from ion conducting components. Rozain and Millet (2014) measured the metallic components to be approximately $120\text{-}150\text{m}\Omega\text{ cm}^2$. For simplicity, the average of $135\text{ m}\Omega\text{ cm}^2$ was used. This resistance can be translated into a voltage drop as aforementioned in conjunction with the MEA area and applied current. R_{el} is the ionic resistance, which corresponds to the ionic conductivity of the electrolyte. Rozain and Millet (2014) measured

the ionic resistance to be 100-130m Ω cm², corresponding to a typical 50-200 μ m thick Nafion® MEA. Similarly to the ohmic resistance, the ionic overpotential can be correlated with respect to MEA area and applied current. Z_D represents the diffusion impedance due to mass transport limitations of gas travelling away from the electrode-electrolyte interface and through the porous transport layer for the cathode and anode, represented by diffusion overpotential, $\eta_{diffusion}$. Millet et al. (2011) performed EIS analysis on a PEMEC to characterize mechanisms of the multi-step charge transfer process, to differentiate the different impedance contributing mechanisms, and found that the impedances are real at low frequencies, suggesting no imaginary (i.e., capacitive-like impedance) contribution (Millet, 2011). Low frequency EIS responses are diffusion dominated mechanisms. This indicates that mass transport impedances are fully developed quickly and therefore have very little capacitive influence and can therefore be neglected. R_{ct} and Z_{dl} correspond to the impedance contribution of charge transfer and electric double layer effects, culminating together to correspond to the activation overpotential, $\eta_{activation}$, which can be approximated using the Butler-Volmer equations. This parameter is non-linear due to the capacitive behaviour of charge transfer resistance and electric double layer effects. These elements correspond to the irreversible losses associated with the electrolyte-electrode interface.

$$\eta_{ohmic}^x = 0.135(iA), x = a, c \quad (3.13)$$

$$\eta_{activation}^x = \frac{RT}{F} \sinh^{-1} \left(\frac{i}{2i_{o,x}} \right), x = a, c \quad (3.14)$$

$$\eta_{diffusion}^x = 0, x = a, c \quad (3.15)$$

$$\eta_{electrolyte}^x = 0.115(iA), x = a, c \quad (3.16)$$

$$E_{applied} = E_0 + \frac{RT}{2F} \ln \left(\frac{\sqrt{P_{O_2}} P_{H_2}}{P_{H_2O}} \right) + \left(\sum \eta \right) \quad (3.17)$$

Further analysis for optimizing cell performance involves EIS analysis to breakdown real and imaginary impedances, corresponding to resistive and capacitive components. These impedances are desired to be minimized to optimize cell performance. The area specific resistance (ASR) is an important parameter influencing electrode performance as it relates the electrode chemical properties with respect to oxygen permeability and conductivity.

In summary, much of these losses are related to high current density operation, as indicated by the equations above, contributing towards the various forms of overpotential. For this reason, power supply and electrode area should be closely considered as these determine the degradation rate of the cell. Furthermore, high current density also introduces higher rates of degradation, which will be later discussed, further deterring high current operation. Another issue associated with excessive current and/or high-pressure operation considers water transport through the membrane (Awasthi, 2011). Any transport of compounds other

than hydrogen ions through the membrane are defined as non-ideal operation due to the increased consumption of energy per unit of hydrogen. The first transport mechanism of water through the membrane is diffusion, which is caused by a concentration gradient on either side of the membrane. This mechanism is for the most part unavoidable since the membrane is saturated with water during operation, however as aforementioned, increasing the pressure can reduce the amount of water saturation, by reducing the membrane porosity. To minimize diffusion losses, maintaining steady-state current operation such that sudden concentration gradients are not present, which drive diffusion outlined by Fick's Law, is desired.

The second mechanism is due to a pressure difference across the membrane thereby forcing mass through the membrane. This mechanism can be managed based on Darcy's law which considers the pressure differential, ΔP , permeability, K , and thickness of the membrane, δ . The other parameters describe the density, ρ , viscosity, μ , and molar mass, M , of the water (Awasthi, 2011). This indicates that water transport is inevitable under differential operation, however, it can be minimized with a greater membrane thickness and lower permeability.

$$N_{H_2O} = \frac{KA\rho_{H_2O}\Delta P}{\delta\mu_{H_2O}M_{H_2O}} \quad (3.18)$$

The third and most dominating mechanism is electro-osmotic drag where the H^+ ions, which are desired to be transported through the membrane, drag water molecules with them through the membrane. This transport mechanism mainly depends on the value of the

dimensionless parameter, n_d , which is a fitting parameter, along with the current density, i , MEA surface area, A , and Faraday's constant, F (A. Awasthi, 2011):

$$N_{H_2O} = \frac{n_d i A}{F} \quad (3.19)$$

Note that the electro-osmotic drag transport mechanism is related to current, further discouraging high current operation.

In summary, the above examples of water transport are all undesired aspects that occur under high current density and differential high-pressure operation. The benefit of operating at differential pressure offers a lower cell potential relative to balanced pressure operation (i.e. equal hydrogen and oxygen chamber at high-pressure), since only the hydrogen chamber is at high-pressure. Furthermore, differential pressure operation negates the need for a water pump, since the oxygen side is at atmosphere, however this requires a recombiner most likely due to H_2 migration into O_2 through membrane due to pressure differential.

Chapter Four: Experimental Temperature and Chemical Treatment Effect

This chapter describes experimental execution of studying the electrochemical response of externally applied heat for temperature effect and of chemically treating the titanium anode GDL with HCl for treatment effect. The temperature effect has been studied previously as discussed, as mentioned in Section 3.1. Chemically treating and fabricating methods are discussed in Section 4.2, such there are various methods for treating different parts of the MEA. This treatment study considers the effect of treating the anode GDL with HCl to remove and reduce future passivation layer growth.

4.1 Methods and Materials

A single electrochemical cell was constructed to measure the effect of temperature on electrochemical performance. The cell was constructed from two machined polycarbonate blocks, which were then pressed firmly together to sandwich the MEA and current collectors together. The polycarbonate apparatus was designed to accommodate multiple ports for water injection, gas release and electricity connection. Polycarbonate was chosen due to the translucent characteristics, allowing direct visual feedback of gas production.

The MEA was purchased prefabricated from the Fuel Cell Store, which was a catalyst coated prepared MEA of 3 mg/cm^2 of IrRuO₂ and 3 mg/cm^2 of Pt/C for the anode and cathode, respectively, onto Nafion 115. This MEA was chosen due to its established high stability characteristics of iridium and ruthenium oxide anode and platinum cathode

electrocatalyst, outlined in Section 2.4.2. The MEA was pressed between a titanium and stainless-steel foil/mesh via the polycarbonate housing with gaskets for the anode and cathode compartments, respectively. The titanium and stainless-steel had a porosity and thickness of 53-56%, 0.2-0.3mm, and 34%, 0.21mm, respectively. The stainless-steel mesh was electrically connected and soldered to a copper wire, which was connected to the negative terminal of the power supply, show in Figure 4.1.1. This setup could not be replicated for the anode side due to the inability of the soldering material to bond onto the titanium and due to the highly acidic local environment at this proximity to the anode electrode interface, copper disintegrates. For this reason, a stainless-steel wire was used and was pressed against the titanium mesh, which was then connected to the copper wire at a stable distance away from the anode electrode interface to establish a positive charge connection, shown in Figure 4.1.2.

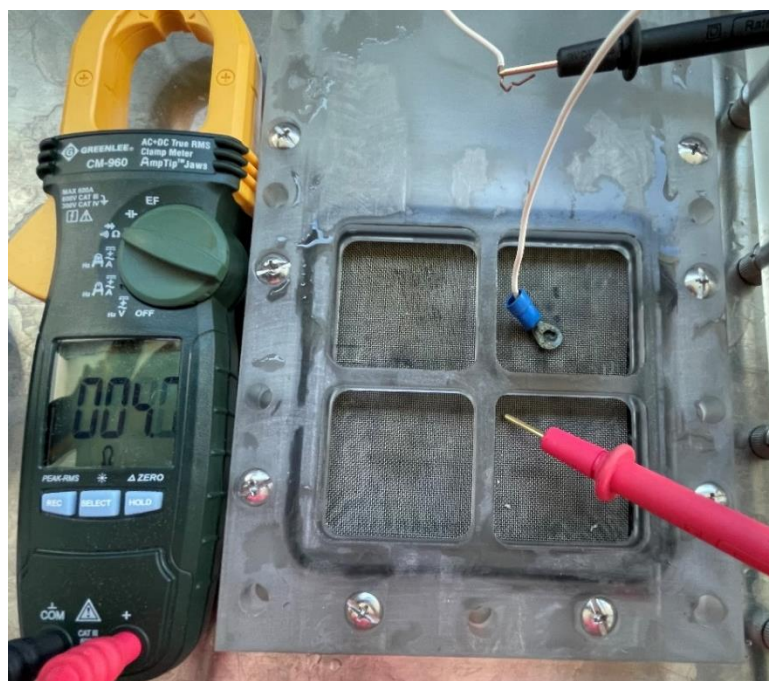


Figure 4.1.1: Cathode GDL and copper wire solder connection.

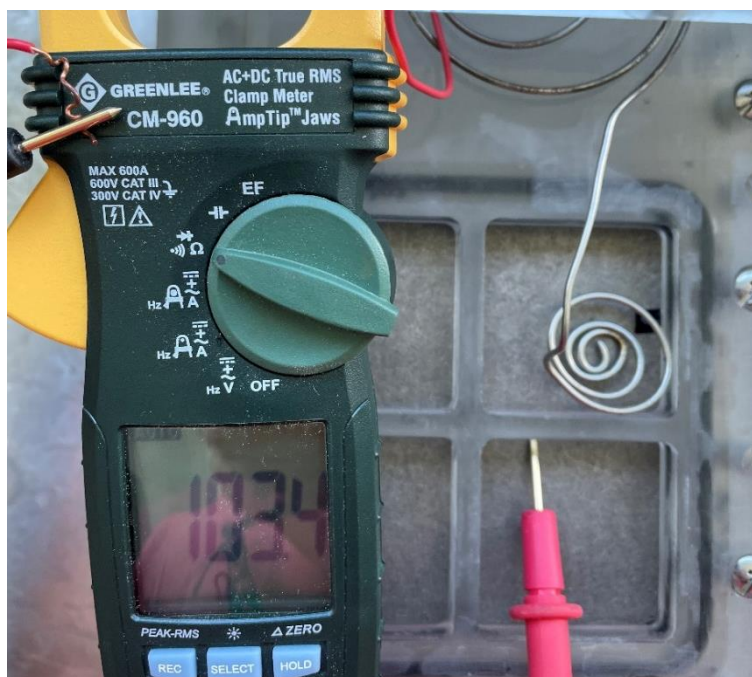


Figure 4.1.2: Anode GDL and in-contact with stainless-steel wire.

An Extech Instruments® DC regulated power supply was used to control the power supply and to convert the laboratory's alternating current (AC) wall outlet into direct current (DC). Mass flow meters supplied from OMEGA® Engineering Inc. were used to measure the oxygen gas and hydrogen gas production rates. Flow measurements were not recorded but used to verify that the reaction was taking place in the proper manner, indicated by Equation (2.1).

The polycarbonate cell was submerged into a water bath that had temperature-controlled circulating water via a VWR™ heating circulator. The temperature of the cell was tested from 10 to 75°C at atmospheric pressure. Furthermore, to verify the purity of the two

respective gas streams such that the measured mass flow rate is measuring the rate of oxygen and hydrogen gas respectively, a GC Agilent was used to verify that the gas streams were of 99.7% purity.

Table 4.1: Recorded flow rates for the following temperature and applied current to verify the correct reaction is taking place based on Equation (2.1) molar ratio.

Temperature	O ₂ Flow Rate	H ₂ Flow Rate	Current
[°C]	[mL/min]	[mL/min]	[mA/cm ²]
15	13.0	26.0	30.0
25	13.0	26.5	30.0
35	12.5	25.5	30.0
45	12.5	26.0	30.0
55	13.0	26.0	30.0
65	13.0	26.0	30.0
75	13.0	26.0	30.0

4.1.1 Temperature effect: Results

The results of the runs at different temperature are displayed in Figure 4.1.3. This plot illustrates the negative slope of the electrochemical potential in volts with respect to reaction temperature. Both the OCV and voltage at 30 mA/cm² have a negative sloping trend, which agrees with the analytical MATLAB® model prediction, which is also plotted. The comparison reveals that the model provides an excellent representation of the experimental results.

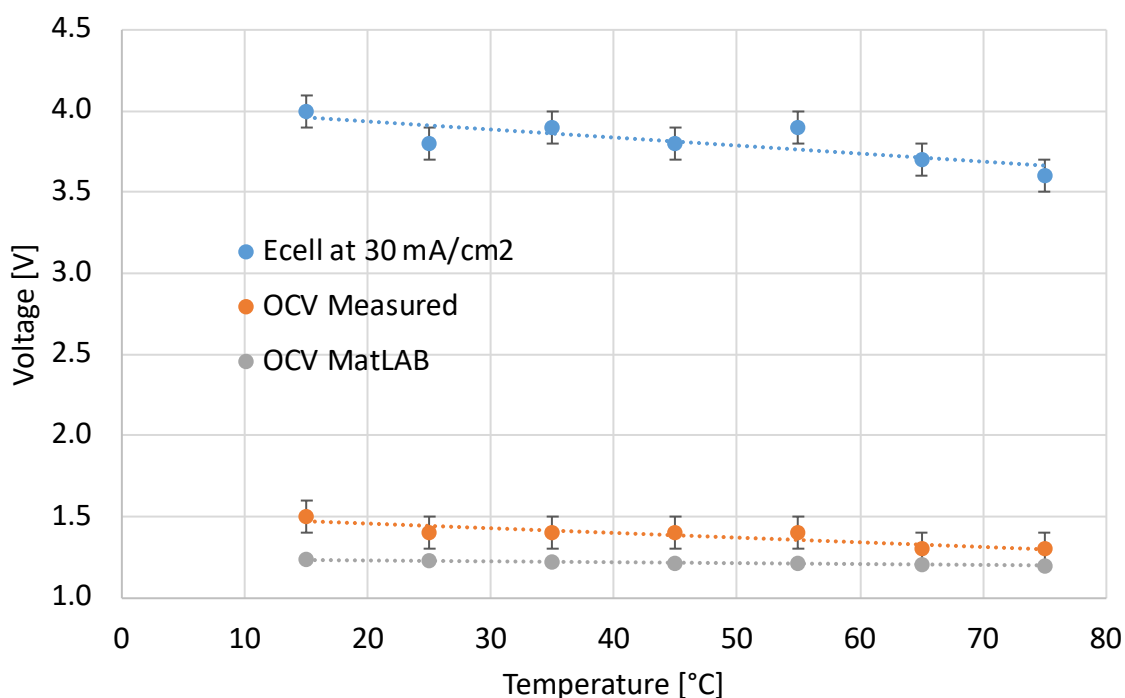


Figure 4.1.3: Temperature effect on the electric potential at onset current and 30mA/cm². As well, the electric potential produced from the analytical model for onset current is plotted for comparison.

The faradaic reaction efficiency was determined by the ratio of the measured and the MATLAB® potentials at OCV, shown below in Equation (4.1) and with experimental and model results displayed in Figure 4.1.4. The faradaic efficiency refers to the percentage contribution of actual vs. theoretical product yield per unit of energy. In this case, the unit of energy and product yield is zero since the OCV is the potential that the reaction starts, indicating that the current is near zero and therefore the product yield is in turn near zero. This ratio outlined above in this case can also refer the faradaic efficiency at OCV. The trend illustrates an increasing efficiency with increased temperatures, which agrees with previous research. The efficiency increase under higher temperatures is attributed towards better reaction kinetics. These transport phenomena include but are not limited to liquid

reactants, product gas, and ion transport, through the GDL and electrocatalyst interface, respectively.

$$\eta_{faradaic} = \frac{E_{reversible}}{E_{irreversible}} = \frac{V_{MATLAB}^{\text{®}}}{V_{measured}} \quad (4.1)$$

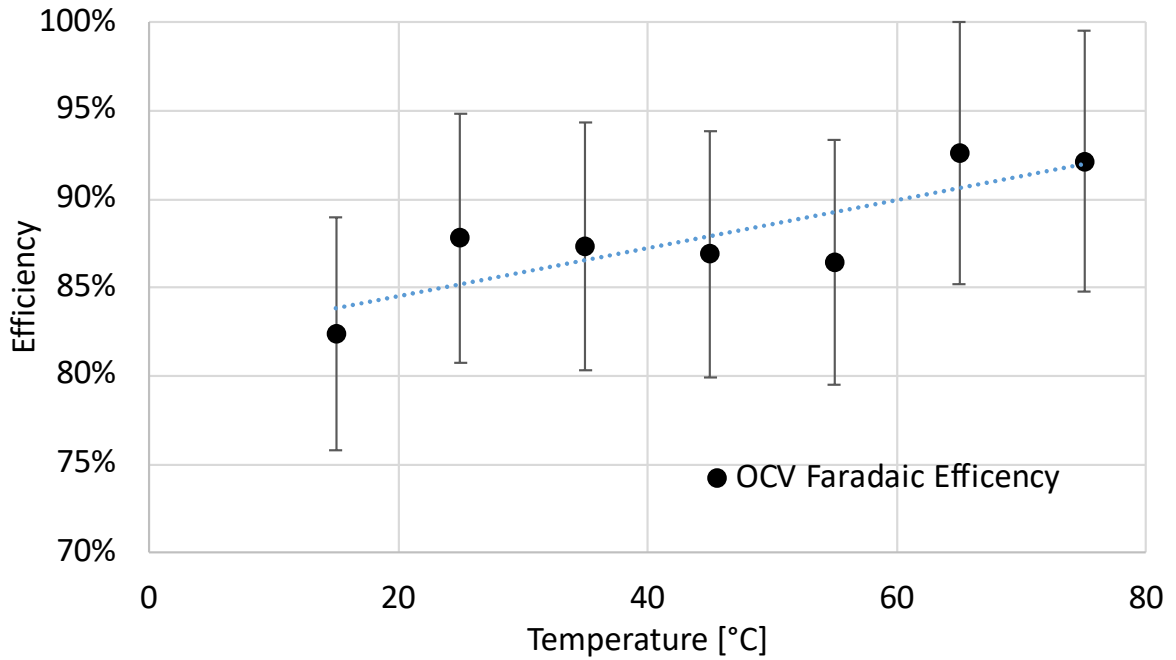


Figure 4.1.4: Electrochemical efficiency of cell with respect to temperature at OCV.

The efficiency of the cell was not determined for 30 mA/cm² since there are many unknown and uncertain irreversible losses associated with this setup for both the actual and theoretical model. Furthermore, even if the theoretical MATLAB[®] model considered irreversible losses, the efficiency would remain considerably low since the actual cell performed very poorly at the relatively higher current density of 30 mA/cm², which should be noted that this is a low current density. Miller et al. (2020) noted that PEMECs generally operate at 2.1V at 2,000 mA/cm² and 50-80°C (Miller et al., 2020). Reasons behind why

the cell performed poorly during the relatively higher current density operation will be discussed below.

It is well established based on the statements above that temperature influences the electrical potential of an electrochemical reaction, such that there is a decrease in electric potential alongside a temperature increase. These changes are attributed due to a lower Gibbs free energy and increased reaction kinetics at higher temperatures.

4.1.2 Temperature Effect: Discussion

Kumar and Himabindu (2019) outlined many MEA configurations, which involved different elemental electrocatalyst combinations, loading amounts, and membrane and membrane thicknesses, such that they all demonstrated an electric potential between 1.6 – 1.9 V at 1.0 A/cm² (Kumar and Himabindu, 2019). These results are on par with what Miller et al. reported, and many others, for expected general PEMEC performance. These performances however are all better than what was observed with the MEA setup in the lab, shown by the polarization results, Figure 4.1.5. The polarization demonstrates the cell's performance on an applied current basis relative to voltage. In an isentropic system, there would be no voltage change relative to current change. However, due to irreversible losses, the voltage increases due to the respective losses discussed in the embodiments concerning. For the observed cell in the lab, the OCV performance was reasonable since it was near the irreversible Nernst potential, which is promising. However, after increasing

the current up to 30 mA/cm², the cell increases in voltage dramatically, indicating significant transport and/or charge transfer resistance are present.

The measured OCV, shown in Figure 4.2.1, reduces at a slightly faster rate than the calculated MATLAB® OCV. This is likely due to the fact that the MATLAB® OCV analytical model does not account for impedances, although in theory, impedances should not affect the OCV since the current is near zero. However there would be some presence of discrepancy due to some current flow. This discrepancy would explain why the two lines are not on top of each other and why the slopes are different with respect to temperature. As temperature increases, the kinetic portion of the subtle impedance presence would be reduced, thereby bringing the MATLAB® and measured OCV closer.

The chosen MEA was a catalyst coated 3 mg of IrRuO₂ and 3 mg of Pt/C for the anode and cathode, respectively, onto Nafion® 115. The loadings concerning this MEA is among the highest loadings that are commonly tested on other research concerning PEMECs. These loading amounts far exceed the minimum threshold for loading adequacy in terms of degradation and performance (Siracusano, 2017, Lettenmeier, 2016). As a result of this, the source of under-performance is likely not due to the MEA. Drawbacks associated with higher loading catalysts involve higher capital costs, and fortunately marginal better stability and efficiency relative to lower loading catalysts (Siracusano, 2017). Secondly, the degradation is considered to be near minimal for this MEA due to the high stability characteristics of the electrocatalysts and membrane in terms of their chemical makeup (Siracusano, 2017). Ruthenium/iridium, platinum, and Nafion® based anode, cathode and

membrane have been widely demonstrated as effective choices for PEMEC testing and operation.

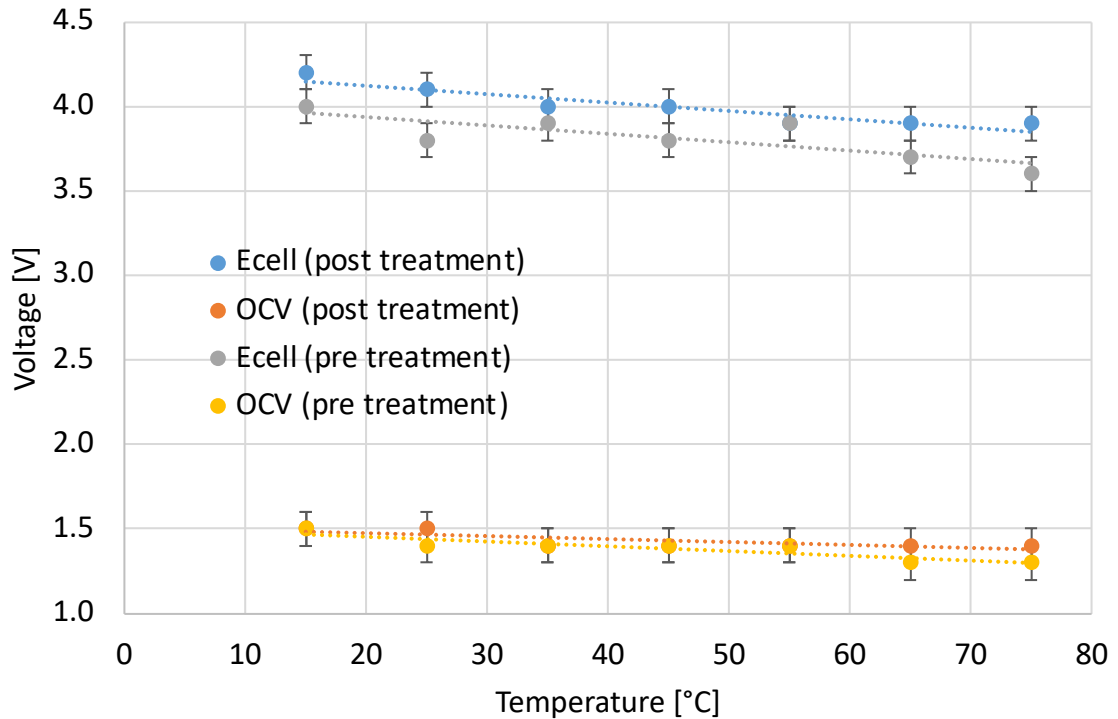


Figure 4.1.5: Post treatment cell potential and OCV results with pre-treatment results.

The titanium and stainless-steel was chosen for the respective GDLs based on stability characteristics, which are well established and agreed, since majority of PEMECs include these materials for their respective GDLs. However, there is reasonable evidence that chemically treating the titanium GDL could offer better performance, based on the frequency of demonstrated preparation methods, respectively. For this reason, the polarization curve tests will be rerecorded to see a potential change of performance after treating the titanium GDL.

4.2 Chemical Treatment

In attempts to improve the performance of the cell to approach polarization results from other published cell performances, the titanium mesh was treated to help remove any pre-existing and reduce the future formation of titanium oxide on the outer surface. According to Byrstron et al. (2018), treating the titanium with hydrochloric acid can remove and significantly delay the growth of the layer of titanium dioxide, which acts as an electrically insulating barrier between the GDL and electrocatalyst (Bystron, 2018).

The treatment process in lab was modified however in accordance with available resources. The titanium mesh was washed with acetone and 2-propanol, then rinsed multiple times in deionizer water. Then the mesh was placed in a 18% HCl solution for 30min at 50°C approximately. This step was lengthened due to the lower concentration of solution available, relative to the recommended 35% HCl for 5 minutes at 54°C. The assembly was reassembled to determine whether the treatment process changed performance. Ultimately indicating the presence and hindrance of TiO₂ outer insulative layer.

4.2.1 Chemical treatment: Results

The cell potential at 30 mA/cm² and open circuit voltage readings were taken again to determine whether the treatment on the titanium mesh had an effect on the performance. Interestingly both the cell potential and OCV post treatment were higher than the values

recorded before treatment. This indicates a performance drop instead of the anticipated and desired performance increase.

Similarly, the OCV efficiency can be determined with respect to the theoretical MATLAB® potential, using Equation (4.1). The efficiency after treatment did not increase at the same rate relative to the efficiency increase before treatment, with respect to temperature.

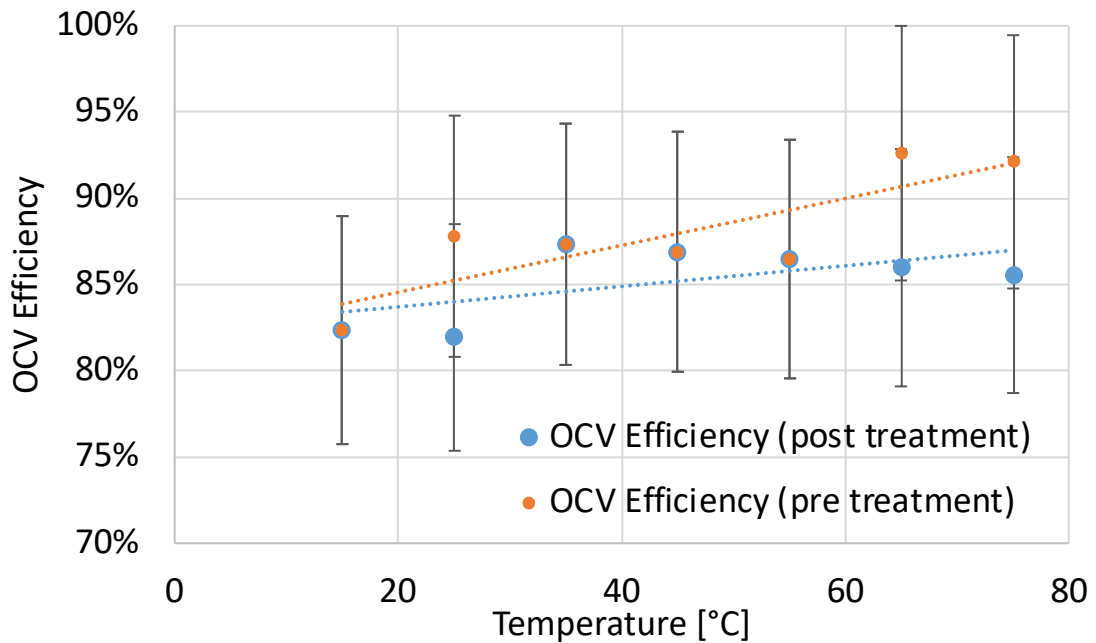


Figure 4.2.1: Post-treatment and pre-treatment OCV faradaic efficiency comparison.

4.2.2 Chemical treatment: Discussion

The treatment did not induce a positive performance change but rather caused a drop in performance. This drop in performance is represented by a higher cell potential for both

the voltage at $30\text{mA}/\text{cm}^2$ and open circuit voltage (OCV), shown in Figure 4.2.1, for all temperature readings. Concerning the voltage at $30\text{mA}/\text{cm}^2$, the slope due to voltage demand change with temperature increase of both the pre-treatment and post-treatment are very similar. This indicates that whatever change occurred while disassembling, treating the titanium, and reassembling the assembly, can be represented by a constant and real impedance.

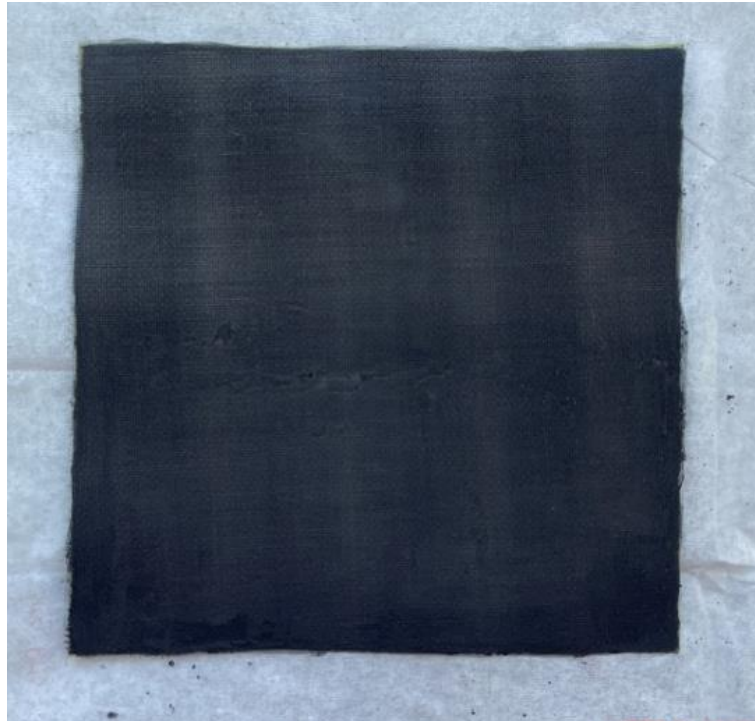
Judging the MEA upon reassembly (i.e. assembling after GDL treatment), with respect to the condition before all testing, the MEA had become increasingly wrinkled. The wrinkling observed is likely because the MEA was not submerged in water during the treatment process, causing water content loss and thus wrinkling. The photos below, Figure 4.2.2, show the difference in conditions described.

One potential source for the observed performance drop, as a result of treatment, could be ascribed from the wrinkling transformation of the MEA that occurred during this process. This is because the wrinkling would cause a reduced contact area between the MEA and the two GDL metal meshes. The wrinkling, due to the membrane drying, would reduce the contact surface area between the relatively two-dimensional flat metal meshes, thus increasing the contact resistance, which is a real impedance and source of reducing the overall performance.

As illustrated in Figure 4.2.1, the efficiency increase with temperature post-treatment was not as high as the efficiency increase with temperature pre-treatment. The discrepancy

between the different rates of efficiency increase, with respect to temperature, between the before and after treatment setups, infer that there is likely an introduced transport related hinderance. In theory and to which what was measured, as temperature increases, the kinetics improve, thus assisting the thermodynamics of the reaction and offering lower cell potential and higher efficiency. Similarly, supporting the notion that the wrinkling of the MEA is the culprit to a performance drop, the post-treated assembly demonstrated higher cell potentials, thus pointing towards some sort of newly introduced real impedance, which could come in the form as a contact resistance impedance. If this is the case, an increase in contact resistance would also influence the kinetics which would ultimately reduce the reaction efficiency.

A



B

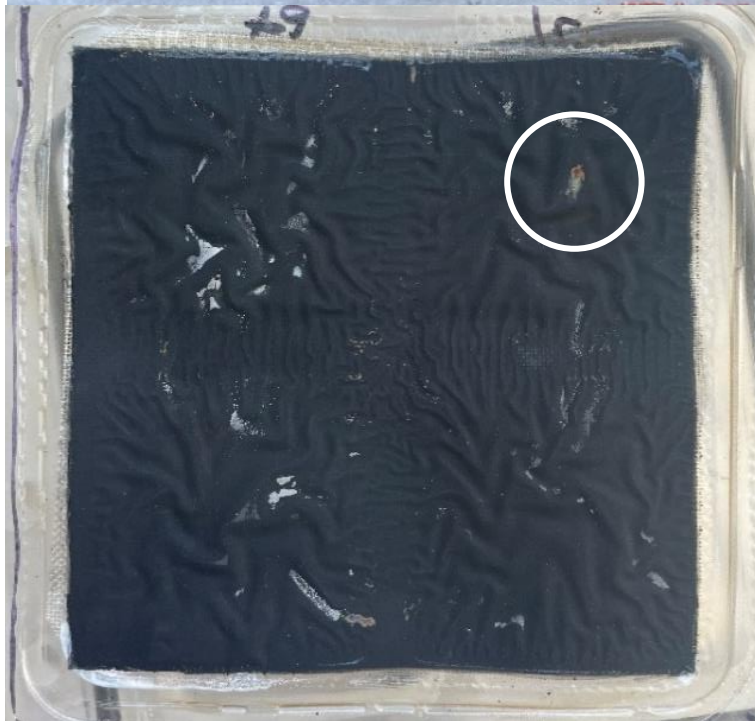


Figure 4.2.2: MEA [A] is the condition of the MEA before all testing. This MEA has not yet been pressed between the GDLs nor submerged in water. MEA [B] is after the first round of testing.

Interestingly, during the disassembly of the cell for treatment, sign of concentrated electrochemical wear was shown on the anode electrocatalyst. This wear is shown in Figure 4.2.2, Image B, indicated by the circle. The wear is located in the same location to where the stainless-steel coil makes contact with the titanium GDL, illustrated in Figure 4.1.2. Electrical connection between the titanium mesh and stainless-steel coil was verified, suggesting electrical conductivity between the titanium mesh and anode catalyst, except for issues mentioned regarding post-treatment testing (i.e. wrinkling), was functioning. Apart from the visible iron deposits on the iridium catalyst, no other conclusions were made to determine the associated effect on performance. EIS would be necessary to determine impedance contributions, in this case, specifically the contact resistance.

Further testing with a thicker titanium GDL is recommended to ensure a larger distance from the anode electrocatalyst interface and stainless-steel material to avoid iron depositing onto the iridium catalyst. In addition, a solid stainless-steel plate should be experimented with since this is common practice.

Losses could be ascribed here as it is common practice to hot-press the MEA and GDL/current collectors together for better contact (Siracusano, 2017). Titanium annealing onto IrO₂ is apparently a critical process to uphold insulating TiO₂ growth and better contact on assembly (Shan, 2015). As well, to introduce a better electrical connection between the circuit and GDL, a thicker GDL would be suitable to facilitate the distance necessary to allow a concentration gradient between the electrocatalyst interface and circuit connection.

4.3 Testing Prefabricated Cell

In attempts to further understand reasons why our cell does not perform as well as other published performances, a prefabricated cell from the Fuel Cell Store was purchased for testing and examination. The cell was submerged in the heated water bath to test the performance over a similar temperature range as tested before for comparison. Once tested, the cell was disassembled to reveal how the cell components were configured to help explain the discrepancies in performance between the two cells.

4.3.1 Prefabricated Cell Results

The prefabricated cell, otherwise referred to as the new cell, demonstrated increased performance results (i.e. lower cell potential) at the 30 mA/cm² current density relative to the in-house built cell at 30 mA/cm². Furthermore the cell potential did not increase significantly when the current density was increased to 76 mA/cm² for the new cell. Interestingly however, the cell potential for the new cell at OCV was higher than the in-house built cell for all temperatures measured. These results are illustrated below in Figure 4.3.1. This means upon start-up, at the onset potential of current (i.e. reaction onset), the new cell offered a lower cell performance relative to the in-house built cell. The reason for this considers overpotential mechanisms that are present upon start-up, which consider activation overpotential. Whereas for the higher current density operation, irreversible processes are dominated by charge-transfer and polarization resistances.

The performance (i.e. cell potential) of the new cell at 76 mA/cm^2 is similar to the in-house built cell at 30 mA/cm^2 , at higher temperatures. This trend is likely to continue such that the difference in performance between the two cells is likely to drift apart, thus further complimenting the performance of the new cell. This means the new cell has a higher sensitivity to the relationship of cell potential reduction and temperature increase. After taking the cell apart, this discrepancy between the in-house built cell and new cell is likely to be due to contact resistances, which are affected by transport related mechanisms.

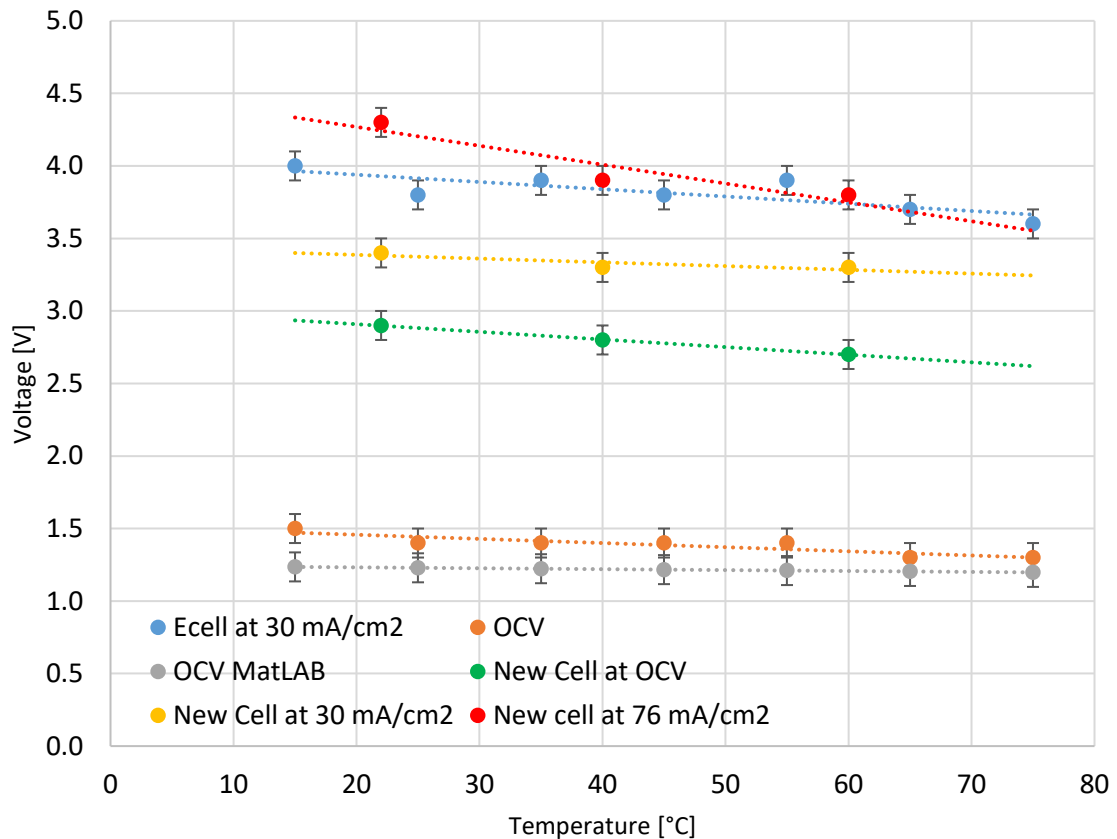


Figure 4.3.1: Performance results with respect to temperature of the new cell and previously in-house tested and built cell.

4.3.2 Prefabricated Cell Disassembly

The prefabricated cell, otherwise referred to as the new cell, was disassembled after testing to understand the configuration of the cell components. More specifically, the goal here was to identify and understand any differences between the two cells that may affect resistances.

The GDLs of the new cell involved multiple layers of meshes with variable porosities which were placed between the catalyst layer (i.e. outer MEA layer) and current collector plates. This approach is similar to the cell made by SENZA Hydrogen Energy and Environmental Technology Co. The endplates of this cell are designed to provide a tight and even pressing contact between each layer of the MEA, GDLs and current collector to cumulatively contribute towards better contact resistance and even usage of catalyst areas. The respective layer components are shown in Figure 4.3.2.

In addition to performance, the in-house built cell suffered from gas leakage issues since the metal compression fit fittings caused the polycarbonate housing to crack, and in turn allowed the produce gas to leak. The new cell was a double circular cell stack, encased in two circular metal endplates of 13.8 cm diameter. The two active areas of the MEAs had an electrocatalyst area of 5 cm diameter. The specifications of the electrocatalyst layers for the new cell were limited to only outlining that precious metals were used for catalyst layers, such that there was no disclosure of loadings and specific elemental compositions. The common IrRuO₂ and Pt/C are common PEMEC catalyst layers and are all considered

precious metals, indicating that the catalysts are the same but no guarantee as the information was not accessible. The large diameter difference between endplate and active area allowed for wide circular gaskets and large bolt fittings around the perimeter to provide the appropriate gas-tight seal.

For the new cell, the gas produced flowed through serpentine-like channels that included small channels between the respective electrode GDL. These channels were around a millimeter wide and high. This small area could explain why the in-house built cell demonstrated better OCV than the new cell. Furthermore, the unknown loadings and composition of the layers could have a hand in the OCV performance, since low loadings and non-PGM metals would reduce performance. Since the new cell includes very small gas channels, bubble transport from the catalyst layer to the exiting tubes could be more difficult compared to the in-house built cell, which allows facile bubble transport from the catalyst layer. The gas channels associated with the new cell are so small that hydrogen transport is likely limited to hydrogen diffusion through the water since these channels are too small for gas bubble transport. This transport mechanism is driven by concentration gradients which is likely much more resistance than buoyancy of bubbles rising away from the catalyst layer for the in-house built cell.

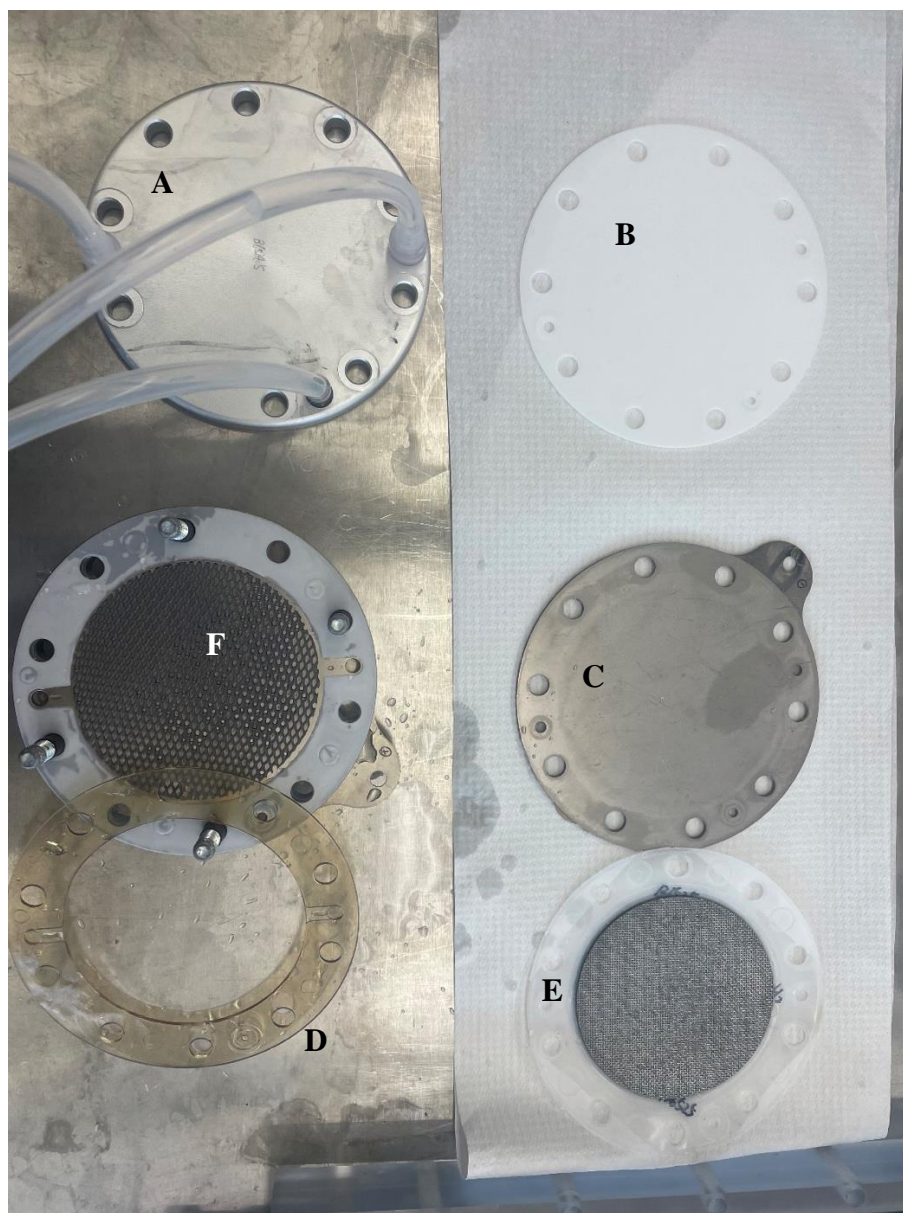


Figure 4.3.2: Image of disassembled cell components of the new cell. See Table 4.2 for description and each component.

Table 4.2: List and description of cell components shown in Figure 4.3.2 of the new cell.

Cell Component	Component Description
A	Metal endplate. Provides the necessary compression amongst cell layers, proper tight gasket seals, and tight compression fit fittings.
B	Electrically insulating film. Inhibits electrical conduction between endplate and current collector.
C	Current collector plate. Facilitates the electrical connection between current supply wires and respective GDLs. This component must withstand corrosive environment.
D	MEA spacer and oxygen gas channel outlets.
E	MEA
F	Gasket and anode GDL.

Chapter Five: Conclusions and Recommendations

In this work, the relationship between temperature and electrochemical performance concerning hydrogen production via electrolysis was tested. The tested cell was considered to be an efficient in-lab assembled proton exchange membrane electrolysis cell (PEMEC), based on the high proton conducting membrane, Nafion®, and the two electrocatalysts which offered low activation energy barriers and high stability. The overall conclusions from the research documented in this thesis are as follows:

1. The measured results and analytical MATLAB® model satisfied each other such that increasing the reaction temperature brought along an increase in electrochemical performance (i.e. cell potential reduction). The benefits associated with a higher reaction temperature is assumed to provide better kinetics and a larger contribution of thermal energy input towards the reaction energy demand, thereby reducing the electricity energy demand (i.e. cell potential) for the reaction.
2. Albeit the effective temperature response, the in-house tested cell did not meet similar performances relative to other published cell performances nor the prefabricated purchased cell. This is indicated by the relatively high cell potential at 30 mA/cm². Significant unknown sources of impedances were present with the tested in-house cell based on the high voltage demand at low current densities. One source of discrepancy between the in-house tested cell and nearly all published cells consider the lack of thermal treatment of the MEA before operation.

3. Chemically treating the membrane did not result in performance increase, in contrast to what Bystron et al. reported. However, the treatment steps were not able to be repeated exactly due to the chemicals available. As well, significant membrane wrinkling took place while the MEA was removed from water during treatment, inducing a non-planar contact between GDL and MEA.
4. Unfortunately, due to inadequate gas seals, high pressure operation was not tested. The cell was designed to structurally withstand up to 2 MPa of pressure build up, to understand the effect on performance. However, the cell would not go about 10 kPa due to leakage.

The following recommendations that arise from this research consider changes to the in-lab cell design to approach already published electrochemical performances:

1. Annealing or hot-pressing is common practice for MEA fabrication by improving the three-phase contact and thus increase performance. The next cell for testing should therefore involve a thermal treatment step during fabrication.
2. To conquer the inadequacies regarding gas-tight seals, the next design should not involve brittle materials for the casing/housing. Tighter bolting forces and tighter press-release fittings are required for high-pressure operation.
3. Bubble interference on mass transport and activation may be a significant issue for scaling up the vertical cell design. Understanding rising bubble interference with respect to the electrocatalyst interface and associated active sites. If bubble

interference is present, offsetting the vertical stack off centre could help to overcome the bubble effect.

4. Testing the cell with multiple anode GDLs in descending wire gage and a solid stainless steel plate instead of the stainless steel wire as the current collectors should be experimented with since this is common practice amongst PEM setups.
5. Consistent testing parameters should be used to properly assess different cell configurations. According to Ayers et al., the United States Department of Energy (DOE) target of 2 A/cm^2 at 1.5 V is equivalent to \$2 per kg of H_2 (K. E. Ayers C. B., 2012). This corresponds to the lower pricing range of \$2-4 per kg of H_2 for electrolysis to become competitive with fossil fuel produced hydrogen (Camillo Spori, 2017). As a result, Fabbri et al. suggested that the activity at 1.5V should be reported to compare MEA configurations and fabricating procedures (E. Fabbri, 2014). In addition, Spori et al. recommended that the activity should also be reported at 2 A/cm^2 to highlight the shortcomings and performance hinderances in the way of eventually reaching the DOEs target (Camillo Spori, 2017). For these reasons, 1.5V and 2 A/cm^2 should be tested as the benchmark parameters for proper comparison.

References

- Aicart, J., Wullemin, Z., Gervasoni, B., Reynaud, D., Waeber, F., Beetschen, C., Antonetti, Y., Nesci, A., & Mougin, J. (2022). Performance evaluation of a 4-stack solid oxide module in electrolysis mode. *International Journal of Hydrogen Energy*, 47(6), 3568–3579. <https://doi.org/10.1016/j.ijhydene.2021.11.056>
- al Shakhshir, S., Cui, X., Frensch, S., & Kær, S. K. (2017). In-situ experimental characterization of the clamping pressure effects on low temperature polymer electrolyte membrane electrolysis. *International Journal of Hydrogen Energy*, 42(34), 21597–21606. <https://doi.org/10.1016/j.ijhydene.2017.07.059>
- Allebrod, F., Chatzichristodoulou, C., Mollerup, P. L., & Mogensen, M. B. (2012). Electrical conductivity measurements of aqueous and immobilized potassium hydroxide. *International Journal of Hydrogen Energy*, 37(21), 16505–16514. <https://doi.org/10.1016/j.ijhydene.2012.02.088>
- Alyssa Bruce, Ariane Bourassa, Daryl Bennett, Grant Strem, Holly Vaughan, Jamie Bonham, Jana Erickson, Juli Rohl, Keely Cameron, Keith Hirsche, Kelley Thompson, Kenryo Mizutani, Lisa Mueller, Liz Lappin, Marla Orenstein, & Yannick Champollion. (2021). *The LEAD Project: Leveraging our Energy Assets for Diversification*.
- Amikam, G., Nativ, P., & Gendel, Y. (2018). Chlorine-free alkaline seawater electrolysis for hydrogen production. *International Journal of Hydrogen Energy*, 43(13), 6504–6514. <https://doi.org/10.1016/j.ijhydene.2018.02.082>
- Aubras, F., Rhandi, M., Deseure, J., Kadjo, A. J. J., Bessafi, M., Majasan, J., Grondin-Perez, B., Druart, F., & Chabriat, J. P. (2021). Dimensionless approach of a polymer

- electrolyte membrane water electrolysis: Advanced analytical modelling. *Journal of Power Sources*, 481. <https://doi.org/10.1016/j.jpowsour.2020.228858>
- Awasthi, A., Scott, K., & Basu, S. (2011). Dynamic modeling and simulation of a proton exchange membrane electrolyzer for hydrogen production. *International Journal of Hydrogen Energy*, 36(22), 14779–14786. <https://doi.org/10.1016/j.ijhydene.2011.03.045>
- Ayers, K. E., Capuano, C., & Anderson, E. B. (2012). Recent Advances in Cell Cost and Efficiency for PEM-Based Water Electrolysis. *ECS Transactions*, 41(10), 15–22. <https://doi.org/10.1149/1.3684798>
- Ayers, K. E., Renner, J. N., Danilovic, N., Wang, J. X., Zhang, Y., Maric, R., & Yu, H. (2016). Pathways to ultra-low platinum group metal catalyst loading in proton exchange membrane electrolyzers. *Catalysis Today*, 262, 121–132. <https://doi.org/10.1016/j.cattod.2015.10.019>
- Babic, U., Suermann, M., Büchi, F. N., Gubler, L., & Schmidt, T. J. (2017). Critical Review—Identifying Critical Gaps for Polymer Electrolyte Water Electrolysis Development. *Journal of The Electrochemical Society*, 164(4), F387–F399. <https://doi.org/10.1149/2.1441704jes>
- Balta, M. T., Kizilkan, O., & Yilmaz, F. (2016). Energy and exergy analyses of integrated hydrogen production system using high temperature steam electrolysis. *International Journal of Hydrogen Energy*, 41(19), 8032–8041. <https://doi.org/10.1016/j.ijhydene.2015.12.211>
- Banas, C. J., Uddin, Md. A., Park, J., Bonville, L. J., & Pasaogullari, U. (2018). Thinning of Cathode Catalyst Layer in Polymer Electrolyte Fuel Cells Due to Foreign Cation

- Contamination. *Journal of The Electrochemical Society*, 165(6), F3015–F3023.
<https://doi.org/10.1149/2.0021806jes>
- Beall, C. E., Fabbri, E., & Schmidt, T. J. (2021). Perovskite Oxide Based Electrodes for the Oxygen Reduction and Evolution Reactions: The Underlying Mechanism. *ACS Catalysis*, 11(5), 3094–3114. <https://doi.org/10.1021/acscatal.0c04473>
- Bo, Y., Wenqiang, Z., Jingming, X., & Jing, C. (2010). Status and research of highly efficient hydrogen production through high temperature steam electrolysis at INET. *International Journal of Hydrogen Energy*, 35(7), 2829–2835.
<https://doi.org/10.1016/j.ijhydene.2009.05.037>
- Brauns, J., Schönebeck, J., Kraglund, M. R., Aili, D., Hnát, J., Žitka, J., Mues, W., Jensen, J. O., Bouzek, K., & Turek, T. (2021). Evaluation of Diaphragms and Membranes as Separators for Alkaline Water Electrolysis. *Journal of The Electrochemical Society*, 168(1), 014510. <https://doi.org/10.1149/1945-7111/abda57>
- Buttler, A., & Spliethoff, H. (2018). Current status of water electrolysis for energy storage, grid balancing and sector coupling via power-to-gas and power-to-liquids: A review. In *Renewable and Sustainable Energy Reviews* (Vol. 82, pp. 2440–2454). Elsevier Ltd. <https://doi.org/10.1016/j.rser.2017.09.003>
- Bystron, T., Vesely, M., Paidar, M., Papakonstantinou, G., Sundmacher, K., Bensmann, B., Hanke-Rauschenbach, R., & Bouzek, K. (2018). Enhancing PEM water electrolysis efficiency by reducing the extent of Ti gas diffusion layer passivation. *Journal of Applied Electrochemistry*, 48(6), 713–723.
<https://doi.org/10.1007/s10800-018-1174-6>

- Carmo, M., Fritz, D. L., Mergel, J., & Stolten, D. (2013). A comprehensive review on PEM water electrolysis. In *International Journal of Hydrogen Energy* (Vol. 38, Issue 12, pp. 4901–4934). <https://doi.org/10.1016/j.ijhydene.2013.01.151>
- Chauveau, F., Mougín, J., Mauvy, F., Bassat, J. M., & Grenier, J. C. (2011). Development and operation of alternative oxygen electrode materials for hydrogen production by high temperature steam electrolysis. *International Journal of Hydrogen Energy*, 36(13), 7785–7790. <https://doi.org/10.1016/j.ijhydene.2011.01.048>
- Corrales-Sánchez, T., Ampurdanés, J., & Urakawa, A. (2014). MoS₂-based materials as alternative cathode catalyst for PEM electrolysis. *International Journal of Hydrogen Energy*, 39(35), 20837–20843. <https://doi.org/10.1016/j.ijhydene.2014.08.078>
- Cropley, C., & Norman, T. (n.d.). *A Low-Cost High-Pressure Hydrogen Generator Final Report*.
- de Pauli, C. P., & Trasatti, S. (n.d.). *Composite materials for electrocatalysis of O₂ evolution: IrO₂ / SnO₂ in acid solution*. www.elsevier.com/locate/jelechem
- Doenitz, W., Schmidberger, R., Steinheil, E., & Streicher, R. (n.d.). HYDROGEN PRODUCTION BY HIGH TEMPERATURE ELECTROLYSIS OF WATER VAPOURt. In *Int. J. Hydrogen Eneroy* (Vol. 5).
- El-Moneim, A. A. (2011). Mn-Mo-W-oxide anodes for oxygen evolution during seawater electrolysis for hydrogen production: Effect of repeated anodic deposition. *International Journal of Hydrogen Energy*, 36(21), 13398–13406. <https://doi.org/10.1016/j.ijhydene.2011.07.100>
- Fabbri, E., Haberer, A., Waltar, K., Kötz, R., & Schmidt, T. J. (2014). Developments and perspectives of oxide-based catalysts for the oxygen evolution reaction. In

- Catalysis Science and Technology* (Vol. 4, Issue 11, pp. 3800–3821). Royal Society of Chemistry. <https://doi.org/10.1039/c4cy00669k>
- Fang, Y. H., & Liu, Z. P. (2010). Mechanism and tafel lines of electro-oxidation of water to oxygen on RuO₂(110). *Journal of the American Chemical Society*, *132*(51), 18214–18222. <https://doi.org/10.1021/ja1069272>
- Felgenhauer, M., & Hamacher, T. (2015). State-of-the-art of commercial electrolyzers and on-site hydrogen generation for logistic vehicles in South Carolina. *International Journal of Hydrogen Energy*, *40*(5), 2084–2090. <https://doi.org/10.1016/j.ijhydene.2014.12.043>
- Fujiwara, S., Kasai, S., Yamauchi, H., Yamada, K., Makino, S., Matsunaga, K., Yoshino, M., Kameda, T., Ogawa, T., Momma, S., & Hoashi, E. (2008). Hydrogen production by high temperature electrolysis with nuclear reactor. *Progress in Nuclear Energy*, *50*(2–6), 422–426. <https://doi.org/10.1016/j.pnucene.2007.11.025>
- Fukuzumi, S., Lee, Y. M., & Nam, W. (2017). Fuel Production from Seawater and Fuel Cells Using Seawater. In *ChemSusChem* (Vol. 10, Issue 22, pp. 4264–4276). Wiley-VCH Verlag. <https://doi.org/10.1002/cssc.201701381>
- Gong, M., Wang, D. Y., Chen, C. C., Hwang, B. J., & Dai, H. (2016). A mini review on nickel-based electrocatalysts for alkaline hydrogen evolution reaction. *Nano Research*, *9*(1), 28–46. <https://doi.org/10.1007/s12274-015-0965-x>
- Grigoriev, S. A., Dzhus, K. A., Bessarabov, D. G., & Millet, P. (2014). Failure of PEM water electrolysis cells: Case study involving anode dissolution and membrane thinning. *International Journal of Hydrogen Energy*, *39*(35), 20440–20446. <https://doi.org/10.1016/j.ijhydene.2014.05.043>

- Grigoriev, S. A., Millet, P., Korobtsev, S. v., Porembskiy, V. I., Pepic, M., Etievant, C., Puyenchet, C., & Fateev, V. N. (2009). Hydrogen safety aspects related to high-pressure polymer electrolyte membrane water electrolysis. *International Journal of Hydrogen Energy*, 34(14), 5986–5991. <https://doi.org/10.1016/j.ijhydene.2009.01.047>
- Grigoriev, S. A., Millet, P., Volobuev, S. A., & Fateev, V. N. (2009). Optimization of porous current collectors for PEM water electrolyzers. *International Journal of Hydrogen Energy*, 34(11), 4968–4973. <https://doi.org/10.1016/j.ijhydene.2008.11.056>
- Grigoriev, S. A., Porembskiy, V. I., Korobtsev, S. v., Fateev, V. N., Auprêtre, F., & Millet, P. (2011). High-pressure PEM water electrolysis and corresponding safety issues. *International Journal of Hydrogen Energy*, 36(3), 2721–2728. <https://doi.org/10.1016/j.ijhydene.2010.03.058>
- Hansen, H. A., Man, I. C., Studt, F., Abild-Pedersen, F., Bligaard, T., & Rossmeisl, J. (2010). Electrochemical chlorine evolution at rutile oxide (110) surfaces. *Physical Chemistry Chemical Physics*, 12(1), 283–290. <https://doi.org/10.1039/b917459a>
- Hinnemann, B., Moses, P. G., Bonde, J., Jørgensen, K. P., Nielsen, J. H., Horch, S., Chorkendorff, I., & Nørskov, J. K. (2005). Biomimetic hydrogen evolution: MoS₂ nanoparticles as catalyst for hydrogen evolution. *Journal of the American Chemical Society*, 127(15), 5308–5309. <https://doi.org/10.1021/ja0504690>
- Hodges, A., Hoang, A. L., Tsekouras, G., Wagner, K., Lee, C. Y., Swiegers, G. F., & Wallace, G. G. (2022). A high-performance capillary-fed electrolysis cell promises

- more cost-competitive renewable hydrogen. *Nature Communications*, 13(1).
<https://doi.org/10.1038/s41467-022-28953-x>
- Huang, K., Hickson, C., Cotterill, D., & Champollion, Y. (2021). Geothermal assessment of target formations using recorded temperature measurements for the Alberta no. 1 geothermal project. *Applied Sciences (Switzerland)*, 11(2), 1–10.
<https://doi.org/10.3390/app11020608>
- IEA. (2019). *The Future of Hydrogen*.
- IEA. (2020). *GREEN HYDROGEN COST REDUCTION SCALING UP ELECTROLYSERS TO MEET THE 1.5°C CLIMATE GOAL H 2 O 2*.
www.irena.org/publications
- Kadakia, K., Datta, M. K., Velikokhatnyi, O. I., Jampani, P., Park, S. K., Saha, P., Poston, J. A., Manivannan, A., & Kumta, P. N. (2012). Novel (Ir,Sn,Nb)O₂ anode electrocatalysts with reduced noble metal content for PEM based water electrolysis. *International Journal of Hydrogen Energy*, 37(4), 3001–3013.
<https://doi.org/10.1016/j.ijhydene.2011.11.055>
- Kadakia, K. S., Jampani, P. H., Velikokhatnyi, O. I., Datta, M. K., Park, S. K., Hong, D. H., Chung, S. J., & Kumta, P. N. (2014). Nanostructured F doped IrO₂ electro-catalyst powders for PEM based water electrolysis. *Journal of Power Sources*, 269, 855–865.
<https://doi.org/10.1016/j.jpowsour.2014.07.045>
- Karimi, F., & Peppley, B. A. (2017). Metal Carbide and Oxide Supports for Iridium-Based Oxygen Evolution Reaction Electrocatalysts for Polymer-Electrolyte-Membrane Water Electrolysis. *Electrochimica Acta*, 246, 654–670.
<https://doi.org/10.1016/j.electacta.2017.06.048>

- Kuang, Y., Kenney, M. J., Meng, Y., Hung, W. H., Liu, Y., Huang, J. E., Prasanna, R., Li, P., Li, Y., Wang, L., Lin, M. C., McGehee, M. D., Sun, X., & Dai, H. (2019). Solar-driven, highly sustained splitting of seawater into hydrogen and oxygen fuels. *Proceedings of the National Academy of Sciences of the United States of America*, *116*(14), 6624–6629. <https://doi.org/10.1073/pnas.1900556116>
- K&z, R., & Stuck1, S. (n.d.). *STABILIZATION OF RuO, BY IrO, FOR ANODIC OXYGEN EVOLUTION IN ACID MEDIA*.
- Lee, J. W., Lee, C., Lee, J. H., Kim, S. K., Cho, H. S., Kim, M., Cho, W. C., Joo, J. H., & Kim, C. H. (2020). Cerium oxide–polysulfone composite separator for an advanced alkaline electrolyzer. *Polymers*, *12*(12), 1–11. <https://doi.org/10.3390/polym12122821>
- Lettenmeier, P., Wang, R., Abouatallah, R., Helmly, S., Morawietz, T., Hiesgen, R., Kolb, S., Burggraf, F., Kallo, J., Gago, A. S., & Friedrich, K. A. (2016). Durable Membrane Electrode Assemblies for Proton Exchange Membrane Electrolyzer Systems Operating at High Current Densities. *Electrochimica Acta*, *210*, 502–511. <https://doi.org/10.1016/j.electacta.2016.04.164>
- Li, N., Araya, S. S., Cui, X., & Kær, S. K. (2020). The effects of cationic impurities on the performance of proton exchange membrane water electrolyzer. *Journal of Power Sources*, *473*. <https://doi.org/10.1016/j.jpowsour.2020.228617>
- Li, N., Araya, S. S., & Kær, S. K. (2019). Long-term contamination effect of iron ions on cell performance degradation of proton exchange membrane water electrolyzer. *Journal of Power Sources*, *434*. <https://doi.org/10.1016/j.jpowsour.2019.226755>

- Liang, Z. X., Zhao, T. S., Xu, C., & Xu, J. B. (2007). Microscopic characterizations of membrane electrode assemblies prepared under different hot-pressing conditions. *Electrochimica Acta*, 53(2), 894–902. <https://doi.org/10.1016/j.electacta.2007.07.071>
- Liu, Z., Sajjad, S. D., Gao, Y., Yang, H., Kaczur, J. J., & Masel, R. I. (2017). The effect of membrane on an alkaline water electrolyzer. *International Journal of Hydrogen Energy*, 42(50), 29661–29665. <https://doi.org/10.1016/j.ijhydene.2017.10.050>
- López-Fernández, E., Sacedón, C. G., Gil-Rostra, J., Yubero, F., González-Elípe, A. R., & de Lucas-Consuegra, A. (2021). Recent advances in alkaline exchange membrane water electrolysis and electrode manufacturing. In *Molecules* (Vol. 26, Issue 21). MDPI. <https://doi.org/10.3390/molecules26216326>
- Lv, H., Zuo, J., Zhou, W., Shen, X., Li, B., Yang, D., Liu, Y., Jin, L., & Zhang, C. (2019). Synthesis and activities of IrO₂/Ti_{1-x}W_xO₂ electrocatalyst for oxygen evolution in solid polymer electrolyte water electrolyzer. *Journal of Electroanalytical Chemistry*, 833, 471–479. <https://doi.org/10.1016/j.jelechem.2018.12.008>
- Mansilla, C., Sigurvinsson, J., Bontemps, A., Maréchal, A., & Werkoff, F. (2007). Heat management for hydrogen production by high temperature steam electrolysis. *Energy*, 32(4), 423–430. <https://doi.org/10.1016/j.energy.2006.07.033>
- Marangio, F., Santarelli, M., & Calì, M. (2009). Theoretical model and experimental analysis of a high pressure PEM water electrolyser for hydrogen production. *International Journal of Hydrogen Energy*, 34(3), 1143–1158. <https://doi.org/10.1016/j.ijhydene.2008.11.083>
- Marshall, A., Børresen, B., Hagen, G., Tsyppkin, M., & Tunold, R. (2005). Preparation and characterisation of nanocrystalline Ir_xSn_{1-x}O₂ electrocatalytic powders. *Materials*

- Chemistry and Physics*, 94(2–3), 226–232.
<https://doi.org/10.1016/j.matchemphys.2005.04.039>
- Mauritz, K. A., & Moore, R. B. (2004). State of understanding of Nafion. *Chemical Reviews*, 104(10), 4535–4585. <https://doi.org/10.1021/cr0207123>
- Mazúr, P., Polonský, J., Paidar, M., & Bouzek, K. (2012). Non-conductive TiO₂ as the anode catalyst support for PEM water electrolysis. *International Journal of Hydrogen Energy*, 37(17), 12081–12088. <https://doi.org/10.1016/j.ijhydene.2012.05.129>
- Miller, H. A., Bouzek, K., Hnat, J., Loos, S., Bernäcker, C. I., Weißgärber, T., Röntzsch, L., & Meier-Haack, J. (2020). Green hydrogen from anion exchange membrane water electrolysis: A review of recent developments in critical materials and operating conditions. In *Sustainable Energy and Fuels* (Vol. 4, Issue 5, pp. 2114–2133). Royal Society of Chemistry. <https://doi.org/10.1039/c9se01240k>
- Millet, P., Mbemba, N., Grigoriev, S. A., Fateev, V. N., Aukauloo, A., & Etiévant, C. (2011). Electrochemical performances of PEM water electrolysis cells and perspectives. *International Journal of Hydrogen Energy*, 36(6), 4134–4142. <https://doi.org/10.1016/j.ijhydene.2010.06.105>
- Mingyi, L., Bo, Y., Jingming, X., & Jing, C. (2008). Thermodynamic analysis of the efficiency of high-temperature steam electrolysis system for hydrogen production. *Journal of Power Sources*, 177(2), 493–499. <https://doi.org/10.1016/j.jpowsour.2007.11.019>
- Neyerlin, K. C., Bugosh, G., Forgie, R., Liu, Z., & Strasser, P. (2009). Combinatorial Study of High-Surface-Area Binary and Ternary Electrocatalysts for the Oxygen Evolution

- Reaction. *Journal of The Electrochemical Society*, 156(3), B363.
<https://doi.org/10.1149/1.3049820>
- Nikiforov, A. v., Petrushina, I. M., & Bjerrum, N. J. (2016). Electrochemical Studies of Corrosion in Liquid Electrolytes for Energy Conversion Applications at Elevated Temperatures. In *High Temperature Corrosion*. InTech.
<https://doi.org/10.5772/64003>
- O'Brien, J. E. (2012). Thermodynamics and transport phenomena in high temperature steam electrolysis cells. In *Journal of Heat Transfer* (Vol. 134, Issue 3).
<https://doi.org/10.1115/1.4005132>
- Onda, K., Kyakuno, T., Hattori, K., & Ito, K. (2004). Prediction of production power for high-pressure hydrogen by high-pressure water electrolysis. *Journal of Power Sources*, 132(1–2), 64–70. <https://doi.org/10.1016/j.jpowsour.2004.01.046>
- Osada, N., Uchida, H., & Watanabe, M. (2006). Polarization Behavior of SDC Cathode with Highly Dispersed Ni Catalysts for Solid Oxide Electrolysis Cells. *Journal of The Electrochemical Society*, 153(5), A816. <https://doi.org/10.1149/1.2177124>
- OWA. (n.d.). *Annual Report 2020/21*.
- Papakonstantinou, G., Algara-Siller, G., Teschner, D., Vidaković-Koch, T., Schlögl, R., & Sundmacher, K. (2020). Degradation study of a proton exchange membrane water electrolyzer under dynamic operation conditions. *Applied Energy*, 280. <https://doi.org/10.1016/j.apenergy.2020.115911>
- Placca, L., & Kouta, R. (2011). Fault tree analysis for PEM fuel cell degradation process modelling. *International Journal of Hydrogen Energy*, 36(19), 12393–12405. <https://doi.org/10.1016/j.ijhydene.2011.06.093>

- Pletcher, D., & Li, X. (2011). Prospects for alkaline zero gap water electrolyzers for hydrogen production. *International Journal of Hydrogen Energy*, 36(23), 15089–15104. <https://doi.org/10.1016/j.ijhydene.2011.08.080>
- Raj, I. A., & Vasu, K. I. (1990). Transition metal-based hydrogen electrodes in alkaline solution-electrocatalysis on nickel based binary alloy coatings. In *JOURNAL OF APPLIED ELECTROCHEMISTRY* (Vol. 20).
- Rakousky, C., Reimer, U., Wippermann, K., Kuhri, S., Carmo, M., Lueke, W., & Stolten, D. (2017). Polymer electrolyte membrane water electrolysis: Restraining degradation in the presence of fluctuating power. *Journal of Power Sources*, 342, 38–47. <https://doi.org/10.1016/j.jpowsour.2016.11.118>
- Rashid, M., al Mesfer, M. K., Naseem, H., & Danish, M. (2015). Hydrogen Production by Water Electrolysis: A Review of Alkaline Water Electrolysis, PEM Water Electrolysis and High Temperature Water Electrolysis. In *International Journal of Engineering and Advanced Technology (IJEAT)* (Issue 3).
- Reytier, M., di Iorio, S., Chatroux, A., Petitjean, M., Cren, J., de Saint Jean, M., Aicart, J., & Mougín, J. (2015). Stack performances in high temperature steam electrolysis and co-electrolysis. *International Journal of Hydrogen Energy*, 40(35), 11370–11377. <https://doi.org/10.1016/j.ijhydene.2015.04.085>
- Rossmesl, J., Qu, Z. W., Zhu, H., Kroes, G. J., & Nørskov, J. K. (2007). Electrolysis of water on oxide surfaces. *Journal of Electroanalytical Chemistry*, 607(1–2), 83–89. <https://doi.org/10.1016/j.jelechem.2006.11.008>
- Rozain, C., Mayousse, E., Guillet, N., & Millet, P. (2016a). Influence of iridium oxide loadings on the performance of PEM water electrolysis cells: Part II - Advanced

- oxygen electrodes. *Applied Catalysis B: Environmental*, 182, 123–131.
<https://doi.org/10.1016/j.apcatb.2015.09.011>
- Rozain, C., Mayousse, E., Guillet, N., & Millet, P. (2016b). Influence of iridium oxide loadings on the performance of PEM water electrolysis cells: Part I-Pure IrO₂-based anodes. *Applied Catalysis B: Environmental*, 182, 153–160.
<https://doi.org/10.1016/j.apcatb.2015.09.013>
- Rozain, C., & Millet, P. (2014). Electrochemical characterization of Polymer Electrolyte Membrane Water Electrolysis Cells. *Electrochimica Acta*, 131, 160–167.
<https://doi.org/10.1016/j.electacta.2014.01.099>
- Santos, A. L., Cebola, M. J., & Santos, D. M. F. (2021). Towards the hydrogen economy—a review of the parameters that influence the efficiency of alkaline water electrolyzers. *Energies*, 14(11). <https://doi.org/10.3390/en14113193>
- Sapountzi, F. M., Gracia, J. M., Weststrate, C. J. (Kees J., Fredriksson, H. O. A., & Niemantsverdriet, J. W. (Hans). (2017). Electrocatalysts for the generation of hydrogen, oxygen and synthesis gas. In *Progress in Energy and Combustion Science* (Vol. 58, pp. 1–35). Elsevier Ltd. <https://doi.org/10.1016/j.pecs.2016.09.001>
- Sato, K., Watanabe, S., Huang, Y., Miyasaka, T., Matsui, T., Yashiro, K., Kawada, T., Amezawa, K., Kumada, K., & Eguchi, K. (2021). Relationship between microstructure and deformation of porous Ni-based cermets under redox cycling. *SN Applied Sciences*, 3(10). <https://doi.org/10.1007/s42452-021-04789-w>
- Schalenbach, M., Carmo, M., Fritz, D. L., Mergel, J., & Stolten, D. (2013). Pressurized PEM water electrolysis: Efficiency and gas crossover. *International Journal of*

- Hydrogen Energy*, 38(35), 14921–14933.
<https://doi.org/10.1016/j.ijhydene.2013.09.013>
- Schalenbach, M., Lueke, W., & Stolten, D. (2016). Hydrogen Diffusivity and Electrolyte Permeability of the Zirfon PERL Separator for Alkaline Water Electrolysis. *Journal of The Electrochemical Society*, 163(14), F1480–F1488.
<https://doi.org/10.1149/2.1251613jes>
- Schalenbach, M., Tjarks, G., Carmo, M., Lueke, W., Mueller, M., & Stolten, D. (2016). Acidic or Alkaline? Towards a New Perspective on the Efficiency of Water Electrolysis. *Journal of The Electrochemical Society*, 163(11), F3197–F3208.
<https://doi.org/10.1149/2.0271611jes>
- Shan, R., Zhang, Z., Kan, M., Zhang, T., Zan, Q., & Zhao, Y. (2015). A novel highly active nanostructured IrO₂/Ti anode for water oxidation. *International Journal of Hydrogen Energy*, 40(41), 14279–14283. <https://doi.org/10.1016/j.ijhydene.2015.04.071>
- Shin, Y., Park, W., Chang, J., & Park, J. (2007). Evaluation of the high temperature electrolysis of steam to produce hydrogen. *International Journal of Hydrogen Energy*, 32(10–11), 1486–1491. <https://doi.org/10.1016/j.ijhydene.2006.10.028>
- Shiva Kumar, S., & Himabindu, V. (2019). Hydrogen production by PEM water electrolysis – A review. In *Materials Science for Energy Technologies* (Vol. 2, Issue 3, pp. 442–454). KeAi Communications Co.
<https://doi.org/10.1016/j.mset.2019.03.002>
- Sigurvinsson, J., Mansilla, C., Arnason, B., Bontemps, A., Maréchal, A., Sigfusson, T. I., & Werkoff, F. (2006). Heat transfer problems for the production of hydrogen from

- geothermal energy. *Energy Conversion and Management*, 47(20), 3543–3551.
<https://doi.org/10.1016/j.enconman.2006.03.012>
- Sigurvinsson, J., Mansilla, C., Lovera, P., & Werkoff, F. (2007). Can high temperature steam electrolysis function with geothermal heat? *International Journal of Hydrogen Energy*, 32(9), 1174–1182. <https://doi.org/10.1016/j.ijhydene.2006.11.026>
- Siracusano, S., Baglio, V., Briguglio, N., Brunaccini, G., di Blasi, A., Stassi, A., Ornelas, R., Trifoni, E., Antonucci, V., & Aricò, A. S. (2012). An electrochemical study of a PEM stack for water electrolysis. *International Journal of Hydrogen Energy*, 37(2), 1939–1946. <https://doi.org/10.1016/j.ijhydene.2011.06.019>
- Siracusano, S., Baglio, V., Grigoriev, S. A., Merlo, L., Fateev, V. N., & Aricò, A. S. (2017). The influence of iridium chemical oxidation state on the performance and durability of oxygen evolution catalysts in PEM electrolysis. *Journal of Power Sources*, 366, 105–114. <https://doi.org/10.1016/j.jpowsour.2017.09.020>
- Siracusano, S., Baglio, V., Lufrano, F., Staiti, P., & Aricò, A. S. (2013). Electrochemical characterization of a PEM water electrolyzer based on a sulfonated polysulfone membrane. *Journal of Membrane Science*, 448, 209–214. <https://doi.org/10.1016/j.memsci.2013.07.058>
- Siracusano, S., Baglio, V., Stassi, A., Merlo, L., Moukheiber, E., & Arico', A. S. (2014). Performance analysis of short-side-chain Aquivion® perfluorosulfonic acid polymer for proton exchange membrane water electrolysis. *Journal of Membrane Science*, 466, 1–7. <https://doi.org/10.1016/j.memsci.2014.04.030>
- Siracusano, S., Baglio, V., van Dijk, N., Merlo, L., & Aricò, A. S. (2017). Enhanced performance and durability of low catalyst loading PEM water electrolyser based on

- a short-side chain perfluorosulfonic ionomer. *Applied Energy*, 192, 477–489.
<https://doi.org/10.1016/j.apenergy.2016.09.011>
- Spöri, C., Kwan, J. T. H., Bonakdarpour, A., Wilkinson, D. P., & Strasser, P. (2017). Stabilitätsanforderungen von Elektrokatalysatoren für die Sauerstoffentwicklung: der Weg zu einem grundlegenden Verständnis und zur Minimierung der Katalysatordegradation. *Angewandte Chemie*, 129(22), 6088–6117.
<https://doi.org/10.1002/ange.201608601>
- Thanasilp, S., & Hunsom, M. (2010). Effect of MEA fabrication techniques on the cell performance of Pt-Pd/C electrocatalyst for oxygen reduction in PEM fuel cell. *Fuel*, 89(12), 3847–3852. <https://doi.org/10.1016/j.fuel.2010.07.008>
- Todd, D., Schwager, M., & Mérida, W. (2014). Thermodynamics of high-temperature, high-pressure water electrolysis. *Journal of Power Sources*, 269, 424–429.
<https://doi.org/10.1016/j.jpowsour.2014.06.144>
- Tong, W., Forster, M., Dionigi, F., Dresp, S., Sadeghi Erami, R., Strasser, P., Cowan, A. J., & Farràs, P. (2020). Electrolysis of low-grade and saline surface water. In *Nature Energy* (Vol. 5, Issue 5, pp. 367–377). Nature Research.
<https://doi.org/10.1038/s41560-020-0550-8>
- Trzeźniewski, B. J., Diaz-Morales, O., Vermaas, D. A., Longo, A., Bras, W., Koper, M. T. M., & Smith, W. A. (2015). In Situ Observation of Active Oxygen Species in Fe-Containing Ni-Based Oxygen Evolution Catalysts: The Effect of pH on Electrochemical Activity. *Journal of the American Chemical Society*, 137(48), 15112–15121. <https://doi.org/10.1021/jacs.5b06814>

- Unnikrishnan, A., Rajalakshmi, N., & Janardhanan, V. M. (2019). Kinetics of electrochemical charge transfer in HT-PEM fuel cells. *Electrochimica Acta*, 293, 128–140. <https://doi.org/10.1016/j.electacta.2018.09.171>
- Vincent, I., Lee, E. C., & Kim, H. M. (2021). Comprehensive impedance investigation of low-cost anion exchange membrane electrolysis for large-scale hydrogen production. *Scientific Reports*, 11(1). <https://doi.org/10.1038/s41598-020-80683-6>
- Wang, M., Wang, Z., Gong, X., & Guo, Z. (2014). The intensification technologies to water electrolysis for hydrogen production - A review. In *Renewable and Sustainable Energy Reviews* (Vol. 29, pp. 573–588). Elsevier Ltd. <https://doi.org/10.1016/j.rser.2013.08.090>
- Wei, G., Xu, L., Huang, C., & Wang, Y. (2010). SPE water electrolysis with SPEEK/PES blend membrane. *International Journal of Hydrogen Energy*, 35(15), 7778–7783. <https://doi.org/10.1016/j.ijhydene.2010.05.041>
- Xu, J., Liu, G., Li, J., & Wang, X. (2012). The electrocatalytic properties of an IrO₂/SnO₂ catalyst using SnO₂ as a support and an assisting reagent for the oxygen evolution reaction. *Electrochimica Acta*, 59, 105–112. <https://doi.org/10.1016/j.electacta.2011.10.044>
- Xu, W., & Scott, K. (2010). The effects of ionomer content on PEM water electrolyser membrane electrode assembly performance. *International Journal of Hydrogen Energy*, 35(21), 12029–12037. <https://doi.org/10.1016/j.ijhydene.2010.08.055>
- Yu, B., Zhang, W. Q., Chen, J., Xu, J. M., & Wang, S. R. (2008). Advance in highly efficient hydrogen production by high temperature steam electrolysis. *Science in*

China, Series B: Chemistry, 51(4), 289–304. <https://doi.org/10.1007/s11426-008-0054-z>

Yuan, X. Z., Zhang, S., Ban, S., Huang, C., Wang, H., Singara, V., Fowler, M., Schulze, M., Haug, A., Andreas Friedrich, K., & Hiesgen, R. (2012). Degradation of a PEM fuel cell stack with Nafion® membranes of different thicknesses. Part II: Ex situ diagnosis. *Journal of Power Sources*, 205, 324–334. <https://doi.org/10.1016/j.jpowsour.2012.01.074>

Zhao, S., Yu, H., Maric, R., Danilovic, N., Capuano, C. B., Ayers, K. E., & Mustain, W. E. (2015). Calculating the Electrochemically Active Surface Area of Iridium Oxide in Operating Proton Exchange Membrane Electrolyzers. *Journal of The Electrochemical Society*, 162(12), F1292–F1298. <https://doi.org/10.1149/2.0211512jes>